

**INFLUENCE OF Ca²⁺ IONS ON FRESHLY
PRECIPITATED CaCO₃ PARTICLES**

**A Thesis Submitted to
the Graduate School of Engineering and Sciences of
İzmir Institute of Technology
in Partial Fulfillment of the Requirements for the Degree of**

MASTER OF SCIENCE


in Chemical Engineering

**by
Olukayode Titus MAJEKODUNMI**

**July 2019
İZMİR**

We approve the thesis of **Olukayode Titus MAJEKODUNMI**

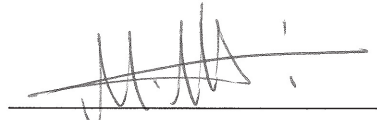
Examining Committee Members:



Prof. Dr. Ekrem ÖZDEMİR
Department of Chemical Engineering, İzmir Institute of Technology

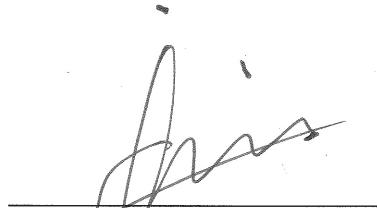


Prof. Dr. Selahattin YILMAZ
Department of Chemical Engineering, İzmir Institute of Technology




Assoc. Prof. Dr. Meral DÜKKANCI
Department of Chemical Engineering, Ege University

1 July 2019



Prof. Dr. Ekrem ÖZDEMİR
Supervisor, Department of Chemical Engineering
İzmir Institute of Technology



Prof. Dr. Erol ŞEKER
Head of the Department of Chemical Engineering

Prof. Dr. Aysun SOFUOĞLU
Dean of the Graduate School of
Engineering and Sciences

ACKNOWLEDGMENTS

To the Supreme One,

To my family,

To Ali Kuşcu Science and Technology Scholarship Program,

To my advisor and professors,

To my friends and colleagues,

To all who contributed to the success of this study,

From the depth of my heart,

I say, THANK YOU.

Sincerely,

Olukayode Titus Majekodunmi.

ABSTRACT

INFLUENCE OF Ca^{2+} IONS ON FRESHLY PRECIPITATED CaCO_3 PARTICLES

The objective of this study was to develop a method to synthesize CaCO_3 nanoparticles from a chemical precipitation reaction under ambient and high supersaturation conditions. Equimolar CaCl_2 and Na_2CO_3 solutions were reacted in a tubular reactor at a constant rate. The particles growth inhibition was attempted by dispersing the reaction mixture in a continuously stirred $\text{Ca}(\text{OH})_2$ solution. This procedure separated the nucleation phase from the growth inhibition process, and was conducted without pH and composition control.

The possibility of impeding the CaCO_3 particles overgrowth was explored at different precipitants and $\text{Ca}(\text{OH})_2$ concentrations. Their effects on the particles morphology, colloidal stability and specific surface area were studied. Although rapidly-settling particles were produced at precipitants concentration of 100 mM, colloidally stable CaCO_3 nanoparticles were obtained at concentrations ≤ 75 mM.

Additive Ca^{2+} ions, provided by the $\text{Ca}(\text{OH})_2$ solutions, inhibited the crystals growth by adsorbing irreversibly on the growth sites. The synthesized particles were as much as 95% smaller than those obtained when pure H_2O was used instead. Ca^{2+} ions concentration and amount of precipitated particles were observed to be important factors for monodispersity and high growth inhibition. Monodisperse and stable nanoparticles were synthesized at low reactants concentration and/or precipitates volume.

Vaterite phase was observed in the particles obtained when pure H_2O was used as the growth-inhibiting solution. However, the presence of additive Ca^{2+} ions effected the crystallization of pure calcite, regardless of $\text{Ca}(\text{OH})_2$ or precipitants concentration, reaction mixtures retention time in the tubular reactor, volume of precipitates, and the growth-inhibiting solutions initial pH.

ÖZET

Ca²⁺ İYONLARININ YENİCE ÜRETİLMİŞ CaCO₃ TANECİKLERİ ÜZERİNE ETKİSİ

Bu çalışmanın amacı, yüksek aşırı doyma ve normal ortam koşullarındaki bir çöktürme reaksiyonundan, CaCO₃ nanotaneceklerini üretmeye yönelik metod geliştirmektir. Eşdeğer molar CaCl₂ ve Na₂CO₃ çözeltileri sabit hızla, tüp şeklinde bir reaktörde reaksiyona sokulmuştur. Yeni oluşan partiküllerin fazla büyümesini engellemek için, reaksiyon karışımı devamlı karıştırılan Ca(OH)₂ çözeltisine dağıtılmıştır. Bu yöntem, çekirdeklenme basamağını, kristal büyümesini engelleme prosesinden ayırmıştır. Kimyasal bileşim ve pH ayarlanmadan tamamlanmıştır.

Üretilen taneciklerin aşırı büyümesinin engelleme olasılığı, farklı Ca(OH)₂ çözeltisi ve tepkenlerin konsantrasyonlarında incelenmiştir. Partiküllerin morfolojisi, koloidal stabilitesi ve özgül yüzey alanı üzerindeki etkiler araştırılmıştır. 100 mM tepken konsantrasyonunda, hızlıca çöken partiküller üretilmesine rağmen, ≤75 mM konsantrasyonlarında kararlı CaCO₃ nanotanecekleri elde edilmiştir.

Ca(OH)₂ çözeltisinden sağlanan katkı Ca²⁺ iyonları, kristallerin yüzeyine geri dönülemez bir şekilde tutunarak aşırı büyümelerini engellemiştir. Sentezlenen tanecikler, Ca(OH)₂ yerine saf H₂O kullanıldığında elde edilenlerden %95'e kadar daha küçüktür. Partiküllerin fazla büyümesinin engellemesi ve homojen boyut dağılımında üretilmesinde, katkı Ca²⁺ iyon konsantrasyonu ve Ca(OH)₂ çözeltisine giren çökeltinin miktarı önemli faktörlerdir. Homojen dağılımlı ve koloidal kararlı kalsit nanotanecekleri düşük çökelti hacmi ve tepkenler konsantrasyonunda üretilmiştir.

Ca(OH)₂ yerine saf H₂O kullanıldığında, taneciklerde vaterit polimorfu elde edilmiştir. Ancak, Ca(OH)₂ veya tepkenlerin konsantrasyonuna, reaksiyon karışımını reaktörde tutma süresine, Ca(OH)₂ çözeltisinin başlangıç pH'ına ve çökelti hacmine bakmaksızın, katkı Ca²⁺ iyonlarının varlığı saf kalsit fazlarının kristallenmesine etki etmiştir.

TABLE OF CONTENTS

LIST OF FIGURES.....	viii
LIST OF TABLES	xi
LIST OF ABBREVIATIONS	xii
CHAPTER 1. INTRODUCTION	1
1.1. Calcium Carbonate.....	1
1.1.1. Polymorphs of CaCO ₃	1
1.1.2. Applications of CaCO ₃	2
1.2. Problem Statement	2
1.3. Aim and Objectives.....	3
1.4. Scope and Limitation.....	3
CHAPTER 2. LITERATURE REVIEW	4
2.1. Structure and Growth of CaCO ₃ Crystals.....	4
2.2. Effects of Additives on CaCO ₃ Crystals.....	6
2.2.1. Enhancement of Particles Properties	7
2.2.2. Crystal Nature	7
2.2.3. Particles Morphology and Synthesis of Superstructures	7
2.2.4. Particles Growth Inhibition	8
2.3. Chemical Precipitation of CaCO ₃ Nanoparticles	9
2.4. Electrical Double Layer and ζ-potential Theory.....	9
2.5. CaCO ₃ Colloidal Stability in Excess Ca ²⁺ Ions Conditions	11
2.6. Why Ca(OH) ₂ ?.....	11
CHAPTER 3. EXPERIMENTAL PROCEDURE	12
3.1. Materials	12
3.2. Experimental Setup	12
3.3. The Tubular Reactor	13

3.4. Studied Parameters.....	14
3.4.1. Residence Time.....	14
3.4.2. Time-dependent Changes in Particle Properties.....	15
3.4.3. Additive Ca ²⁺ ion and Precipitants Concentration.....	16
3.4.4. Growth-inhibiting Solutions initial pH.....	16
3.5. Particle Characterization.....	17
CHAPTER 4. RESULTS AND DISCUSSION.....	18
4.1. Residence Time Effects.....	18
4.2. Evolution of Particle Properties.....	21
4.3. Reaction(s) in the Growth-inhibiting Solution?.....	29
4.4. Adsorption of Additive Ca ²⁺ ions on Particles Surfaces.....	31
4.5. Effects of Ca(OH) ₂ Concentration.....	32
4.5.1. Particle Growth and Colloidal Stability.....	33
4.5.2. Polymorphic Transformation.....	37
4.5.3. Alteration of Particles Morphology.....	38
4.5.4. Changes in Particles Specific Surface Area.....	39
4.6. Precipitants Concentration and Volume Effects.....	41
4.7. Synthesizing Stable Monodisperse Calcite Nanoparticles.....	43
4.8. Stabilizing Solutions Initial pH Effects.....	45
4.8.1. Crystal Form.....	45
4.8.2. Particles Size and Morphology.....	47
4.8.3. Particles Colloidal Stability and Specific Surface Area.....	49
4.8.4. Changes in Suspensions pH.....	52
4.8.5. Changes in Suspensions Conductivity.....	53
CHAPTER 5. CONCLUSION.....	56
REFERENCES.....	58

LIST OF FIGURES

<u>Figure</u>	<u>Page</u>
Figure 2.1. Typical morphology of anhydrous polymorphs of CaCO ₃ : (a) rhombohedral calcite; (b) spherical vaterite; (c) rod-like aragonite.	4
Figure 2.2. Solution-mediated transformation of amorphous CaCO ₃ into calcite at room temperature.	6
Figure 2.3. Morphosynthesis of CaCO ₃ with: (a) <i>N,N</i> -dimethylformamide (DMF); (b) mixture of <i>p</i> -aminobenzene sulfonic acid and <i>L</i> -Lys; (c) poly(ethylene glycol)- <i>b</i> -poly(aspartic acid); (d) poly(styrene- <i>alt</i> -maleic acid); (e) dimethyldioctadecylammonium bromide (DDAB); (f) poly(ethylene glycol)- <i>b</i> -poly(methacrylic acid).....	8
Figure 2.4. Electrical double layer.	10
Figure 3.1. Experimental setup: 1. Na ₂ CO ₃ solution; 2. CaCl ₂ solution; 3. Peristaltic pump; 4. Mixing tee; 5. Tubular reactor; 6. Conductivity probe; 7. pH probe; 8. Magnetic stirrer; 9. Conductivity and pH meter; 10. Computer; 11. Ca(OH) ₂ solution.	13
Figure 4.1. Particles size change during stabilization in 250 mL of 10 mM Ca(OH) ₂ solution: $C_A =$ (a) 25 mM; (b) 50 mM; (c) 75 mM; and (d) 100 mM.	19
Figure 4.2. ζ -potential change during stabilization in 250 mL of 10 mM Ca(OH) ₂ solution: $C_A =$ (a) 25 mM; (b) 50 mM; (c) 75 mM; and (d) 100 mM.	20
Figure 4.3. Particles stabilization in 250 mL of 10 mM Ca(OH) ₂ solution. Effects of C_A on (a) particles size and (b) ζ -potential, when $\tau = 9$ seconds.	21
Figure 4.4. Time-dependent changes in size and ζ -potential of particles stabilized when $C_A = 75$ mM and $\tau = 2$ minutes.	22
Figure 4.5. Time-dependent changes in particles size distribution when $C_A = 75$ mM and $\tau = 2$ minutes.	23

<u>Figure</u>	<u>Page</u>
Figure 4.6. Properties of particles stabilized in ultrapure DI H ₂ O at the 8th minute when $C_A = 75$ mM and $\tau = 2$ minutes: (a) XRD pattern; (b) Morphology and polycrystalline vaterite (inset in b).....	23
Figure 4.7. Time-dependent particles morphology changes when $C_A = 75$ mM and $\tau = 2$ minutes: (a) – (h), 1st – 8th minute respectively.	24
Figure 4.8. Particles Crystal form when $C_A = 75$ mM and $\tau = 2$ minutes.	26
Figure 4.9. Particles surface area analyses for $C_A = 75$ mM and $\tau = 2$ minutes: (a) Time-dependent change in BET SSA; (b) Isotherm linear plot of particles obtained at the 8th minute.	27
Figure 4.10. Time-dependent changes in crystallites average size when $C_A = 75$ mM and $\tau = 2$ minutes	28
Figure 4.11. Conductivity changes during the growth inhibition process when $C_A = 75$ mM and $\tau = 2$ minutes.....	30
Figure 4.12. Time-dependent changes in the solutions cations concentration when $C_A = 75$ mM and $\tau = 9$ seconds.....	31
Figure 4.13. Particles morphology as a function of β and C_S for $C_A = 50$ mM.....	34
Figure 4.14. Morphology change as a function of C_A and C_S for $\beta = 1$	35
Figure 4.15. Morphology change with respect to β for $C_S = 15$ mM.....	36
Figure 4.16. Crystal form with respect to C_S for $C_A = 50$ mM.	38
Figure 4.17. Effects of C_S on particles BET SSA when $\beta = 1$	39
Figure 4.18. Isotherm linear plot of particles synthesized when $C_A = 25$ mM, $\beta = 1$ and $C_S =$: (a) 0 mM; (b) 5 mM; (c) 10 mM; (d) 15 mM.....	40
Figure 4.19. Growth inhibition and morphology change for $C_A = 25$ mM.....	44
Figure 4.20. Particles size distribution for $C_A = 25$ mM: (a) Effects of C_S when $\beta = 0.5$; (b) Effects of β when $C_S = 15$ mM.....	45
Figure 4.21. Crystal form of particles obtained when growth inhibition was attempted in both NaOH solution with initial pH ≈ 13 and pure H ₂ O.....	46
Figure 4.22. Stabilizing solutions initial pH effects on crystals form when $C_A = 25$ mM, $C_S = 10$ mM and $\beta = 0.5$	46
Figure 4.23. Particles hydrodynamic sizes and ζ -potential changes at different pH when $C_A = 25$ mM, $C_S = 10$ mM and $\beta = 0.5$	48

<u>Figure</u>	<u>Page</u>
Figure 4.24. Stabilizing solutions initial pH effects on particles morphology when $C_A = 25$ mM, $C_S = 10$ mM and $\beta = 0.5$. pH = (a) 12.5; (b) 12.0 (c) 11.5; (d) 11.0; (e) 10.0; (f) 9.0.	48
Figure 4.25. Morphology of particles synthesized when growth inhibition was attempted in: (a) NaOH solution with initial pH ≈ 13 ; and (b) pure H ₂ O.	49
Figure 4.26. Particles BET SSA at different initial pH.	50
Figure 4.27. Stabilizing solutions pH changes for different initial pH when $C_A = 25$ mM, $C_S = 10$ mM and $\beta = 0.5$	51
Figure 4.28. Solutions conductivity changes for different initial pH when $C_A = 25$ mM, $C_S = 10$ mM and $\beta = 0.5$	52
Figure 4.29. Relationship between the pH and conductivity of 10 mM Ca(OH) ₂ solution.	53
Figure 4.30. Relationship between Ca(OH) ₂ concentration and conductivity.	54

LIST OF TABLES

<u>Table</u>	<u>Page</u>
Table 3.1. Studied experimental parameters.	14
Table 4.1. ζ -potential and particle size after stabilization and ageing when $\tau =$ 9 seconds.	29
Table 4.2. Particles stability and hydrodynamic sizes.	33
Table 4.3. Particles ζ -potential and hydrodynamic sizes in different stabilizing solutions.	49

LIST OF ABBREVIATIONS

C_A : Precipitants concentration

C_S : Starting concentration of Ca^{2+} ions in growth-inhibiting solution

τ : Precipitates retention time in the tubular reactor

β : Ratio of reaction mixtures volume to the volume of solution used for growth inhibition

SSA: Specific surface area

CHAPTER 1

INTRODUCTION

1.1. Calcium Carbonate

Calcium carbonate (CaCO_3) is a mineral found in abundance on earth: 7% of the earth's crust is estimated to be CaCO_3 ¹. It occurs naturally in geological deposits such as limestone and marble. It is also found in biological systems including: mollusk shells, egg shells and corals. Though it has numerous industrial and technological applications, CaCO_3 precipitates undesirably in heating equipment, resulting in scales formation and reduced efficiency. These, in large part, have made it an extensively studied inorganic mineral². It also serves as a prototype for understanding precipitation processes.

CaCO_3 particles obtained from natural sources by comminution are known as ground calcium carbonate (GCC) while those synthesized in chemical reactions are precipitated calcium carbonate (PCC). Methods of synthesizing PCC can be broadly classified into two: carbonation and chemical method. Carbonation is a heterogeneous phase carbon capture and storage method. It involves the absorption of $\text{CO}_2(\text{g})$ in a solution containing Ca^{2+} ions³⁻⁴. Conversely, chemical synthesis methods are homogenous phase mixing of solutions containing Ca^{2+} and CO_3^{2-} ions.

1.1.1. Polymorphs of CaCO_3

CaCO_3 occurs in both anhydrous and hydrated polymorphic forms. The hydrated forms are $\text{CaCO}_3 \cdot \text{H}_2\text{O}$ and $\text{CaCO}_3 \cdot 6\text{H}_2\text{O}$ while aragonite, vaterite and calcite are anhydrous⁵. CaCO_3 is commonly found in nature as a mixture of its polymorphs. A polymorph might predominate, depending on the solutions conditions. The transformation of CaCO_3 polymorphs is a solution-mediated process, and follows Ostwald's Rules of Stages. The least soluble phase first precipitates, dissolves and simultaneously recrystallizes into a more stable form⁶⁻⁹. Calcite is the most thermodynamically stable polymorph.

1.1.2. Applications of CaCO₃

CaCO₃ has several applications besides its use in cement production. Its availability and low cost has led to its growing global demand, which surpassed 113 million tons in 2016 and estimated to reach 180 million tons in 2025. Also, the global market size was valued at ~\$21 billion in 2016, and expected to worth ~\$34 billion in 2025.

CaCO₃ is widely used as a filling material in paper, paint, plastics, polyurethane foams and adhesives. It significantly reduces the cost of production, and improves both physical and mechanical properties of materials¹⁰⁻¹¹. It is a cost-efficient extender used in paints and coatings, a replacement for pigments such as TiO₂¹². It is also applied to enhance the opacity, brightness and print quality of paper¹³.

Due to its nontoxicity and increased solubility in acidic media, CaCO₃ is used in pharmaceutical industries as a calcium supplement and in antacid formulations. Also, it is a cheaper substitute for SiO₂ and CaHPO₄ particles, used as abrasives, absorbents and emulsion stabilizers in personal care products such as toothpastes and cosmetics¹⁴. Other applications include: enhancement of the mechanical properties of biomedical implants¹⁴⁻¹⁶; treatment of dermal allergic reactions to Nickel¹⁷; and water treatment¹⁸. CaCO₃ particles are increasingly used in anticancer drug delivery, either as lone carriers or in composites¹⁹⁻²³.

1.2. Problem Statement

A topic of recent intense research activity is the development of methods for controlled synthesis of small materials²⁴. Compared to micron sizes, the use of ultra-small materials, such as nano-CaCO₃, have been shown to better enhance mechanical properties of composite materials²⁵.

CaCO₃ develops high supersaturation required to drive a precipitation process, due to its insolubility. Regardless of the solutes concentration, precipitated CaCO₃ particles also grow rapidly and excessively in aqueous media, especially when no inhibitor is present^{2, 26-28}. This is easily observed in chemical precipitation methods. Unlike carbonation processes, the crystals overgrowth makes the chemical synthesis of CaCO₃ in nano sizes impossible at relatively high precipitants concentration.

Although nano-CaCO₃ particles can be synthesized in carbonation methods, there are safety concerns regarding the handling of pressurized CO_{2(g)}. Also, the cost of producing nano-sized GCC is high, and the particles are rarely homogeneously distributed or free of impurities. Besides the physical properties, the use of CaCO₃ particles is also constrained by its purity^{14, 24, 29-30}. Particles containing trace amounts of radioactive or carcinogenic substances cannot be used in health-related or food packaging applications. Hence the need for a more efficient and safer method to produce nano-CaCO₃ particles.

1.3. Aim and Objectives

The aim of this study was to impede the growth of freshly-precipitated CaCO₃ particles by improving electrostatic repulsions among the crystals, and poisoning their growth sites with additive Ca²⁺ ions. Sequel to a previous study³¹ discussing the potential use of aqueous Ca(OH)₂ as a natural stabilizer for CaCO₃ particles, this study demonstrates a new method of inhibiting the overgrowth of CaCO₃, and synthesis of nanoparticles, by stabilizing precipitates in Ca(OH)₂ solution. Here, equimolar CaCl₂ and Na₂CO₃ solutions were reacted in a tubular reactor and continuously dispersed in stirred Ca(OH)₂ solutions.

An objective was to establish the extent to which the additive Ca²⁺ ions, from Ca(OH)₂ solution, can significantly inhibit the growth of CaCO₃ particles under normal atmospheric conditions and relatively high degrees of supersaturation. Ca(OH)₂ concentration and initial pH, precipitants volume and concentration, and the reaction mixtures residence time in the reactor were varied. Their effects on the particles size, stability, crystal form, specific surface area and morphology were examined. Time-dependent changes in the stated particle properties were also studied. The term *stability* is used here to mean the ζ-potential of the dispersed phase.

1.4. Scope and Limitation

The suspensions pH and composition were not controlled during the experiments. Rather, the process proceeded spontaneously. Low solubility of Ca(OH)₂ in H₂O at ambient temperature was the main drawback that was encountered.

CHAPTER 2

LITERATURE REVIEW

2.1. Structure and Growth of CaCO₃ Crystals

Each polymorph of CaCO₃ exhibit distinct structures. Typically, vaterite occurs as spheres, calcite as rhombohedra, and aragonite are fibers or rod-like. Commonly observed shapes are presented in Figure 2.1. The literature, however, intimates that the polymorphs can be manipulated into diverse fascinating superstructures.

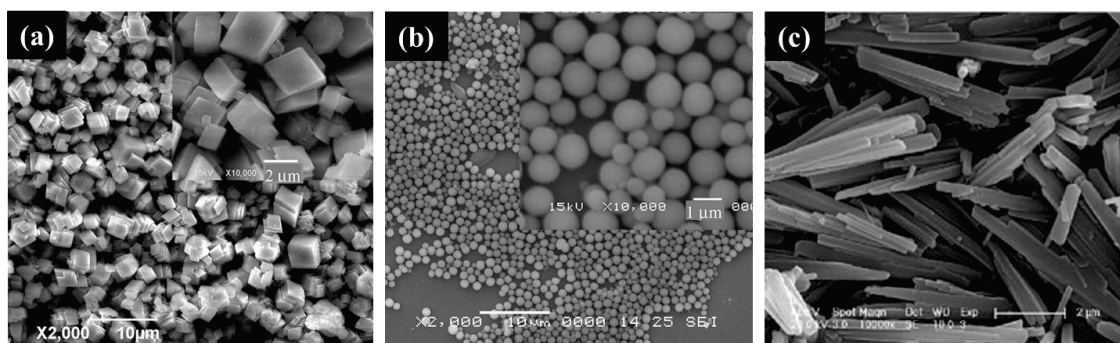


Figure 2.1. Typical morphology of anhydrous polymorphs of CaCO₃: (a) rhombohedral calcite³²; (b) spherical vaterite³²; (c) rod-like aragonite³³.

Precipitation is a fast crystallization process, and the speed is proportional to the degree of supersaturation. CaCO₃ crystallizes easily due to its low solubility, which was found in an earlier study to be ~0.13 mM at 23°C³¹. In the absence of inhibitors, the crystals grow and aggregate in order to minimize their interfacial area to the solution, and achieve equilibrium. Theoretically, precipitation is completed when a crystal comes into equilibrium with the saturated solution. However, in practice, the precipitation process terminates when the crystals attain a critical size that triggers sedimentation.

The crystals growth is a complex process, but there are two basic growth theories. The classical view is that each crystal nucleates in a single event and grows, from the nucleus, by further deposition and assembly of molecules and ions from the solution^{9,34}. In recent years, however, CaCO₃ crystals growth has been argued to be preceded by the

aggregation of prenucleation nano-clusters³⁵⁻³⁶. It is generally accepted that the complex crystal structures exhibited by CaCO₃ challenges the traditional view.

The growth mechanism can differ based on the physical and chemical conditions of the precipitation process. These include: the solutions pH, temperature, precipitation method, and the concentration and properties of foreign substances or counter ions present in the solution. This makes a consensus on CaCO₃ systems problematic^{34, 36-37}. For instance, Andreassen³⁴ argued that vaterite crystals can only grow spherulitically, and not through some prenucleation ion clusters. However, Nehrke and van Cappellen³⁸ pointed out that the result obtained by Andreassen³⁴ was due to the use of a different precipitation method. While the former bubbled CO_{2(g)} in a solution of CaCl₂.H₂O containing NH₃ to synthesize the vaterite particles, the later mixed equal volumes Ca(NO₃)₂ and Na₂CO₃ both containing equimolar NaNO₃.

Several processes occur after the precipitation of CaCO₃. While the crystals are growing, they also undergo polymorphic transformation. The particles instantaneously precipitated upon contact between the solutions containing the lattice ions are highly unstable and poorly-ordered spheres. This amorphous phase rapidly transforms into any of the polymorphs, through several possible ways³⁹⁻⁴⁰. For instance, calcite crystallizes via metastable vaterite phase under normal solution conditions and ambient temperature, but aragonite crystallizes at temperatures ≥ 40 °C^{1, 6, 39}. The period of transformation of unstable and metastable phases into more thermodynamically stable modifications is known as ageing. It is a dissolution-recrystallization process. A schematic representation of the polymorphs transformation process at ambient temperature is presented in Figure 2.2. It shows that while the amorphous phase disappears, the vaterite and calcite concentration increases simultaneously. At longer times, the vaterite phase would have completely recrystallize into calcite.

Solutes concentration is also a key factor affecting the growth of CaCO₃ particles. Under specified conditions of temperature and pressure, from Eq. 2.1 – 2.3, increasing the concentration of any solute ion implies a higher degree of supersaturation, since the solubility product (K_{SP}) is constant. Consequently, the crystals growth rate would increase. By implication, a low concentration of smaller particles would precipitate at lower degrees of supersaturation^{26, 41}.



Saturation index:

$$S = \frac{a_{Ca^{2+}} \cdot a_{CO_3^{2-}}}{K_{SP}} \quad (2.2)$$

a_j is the ionic activity of species j , a product of the activity coefficient and concentration.

Solubility product:

$$K_{SP} = [Ca^{2+}]_{eq} \cdot [CO_3^{2-}]_{eq} \quad (2.3)$$

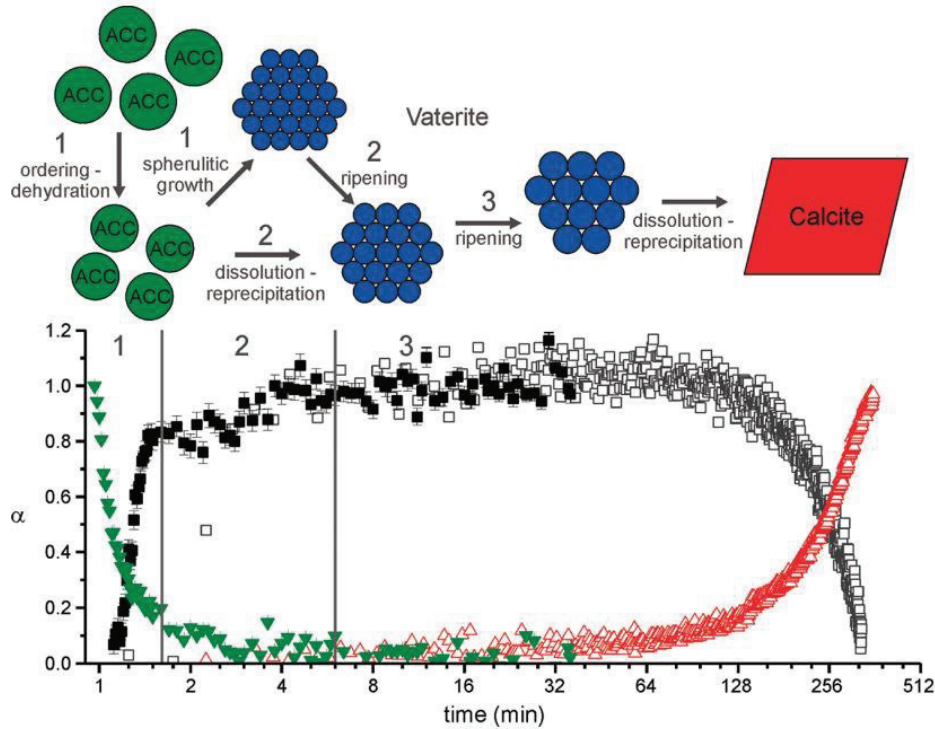


Figure 2.2. Solution-mediated transformation of amorphous $CaCO_3$ into calcite at room temperature (Source: Bots et al. ⁶).

2.2. Effects of Additives on $CaCO_3$ Crystals

The nucleation and growth of $CaCO_3$ structures needed in biosystems is known to be controlled by biomacromolecules ^{35, 42-43}. This has inspired several research efforts, as diverse solvents and polymers have been used to mimic the perceived functions of these biogenics for morphosynthesis of $CaCO_3$ superstructures, and elucidation of its polymorphic transformation in aqueous systems ^{29, 44-49}. Studies show that the incorporation of foreign species into the lattice influences the crystal nature ^{1, 50-52}, growth ^{6, 19, 26, 28-29, 53}, mechanical and physical properties of $CaCO_3$ particles ^{42, 54}.

2.2.1. Enhancement of Particles Properties

The incorporation of foreign species within materials is a valuable way of producing new functional materials with improved physical and mechanical properties. Green et al.⁵⁴ reported that the fluorescence of calcite particles can be tuned by the occlusion of sulfonated fluorescent dyes. The authors reported the dyes were incorporated in specific zones within the crystal lattice. The dyes presence also caused changes in the crystals morphology.

Likewise, Kim et al.⁴² showed the hardness of single-crystal calcite particles can be improved by increasing the concentration of amino acids occluded in their lattices. The incorporated molecules were shown to appear as second phase particles which blocked dislocation motions in the crystals and enhanced their hardness.

2.2.2. Crystal Nature

Calcite is the most thermodynamically stable form of CaCO_3 . However, the presence of impurity ions can affect the polymorphic transition process, influencing the precipitation of specific polymorphs. Manoli and Dalas⁵¹ showed ethanol, isopropanol and diethylene glycol stabilizes vaterite polymorph, and prevents its transformation to calcite. According to Tai et al.¹, Mg^{2+} and Mn^{2+} ions favor the formation of either aragonite or calcite, depending on the impurities concentration, saturation index, solution pH and temperature. Ca^{2+} ions, when present in excess amounts, is known to promote the crystallization of calcite^{1, 3, 27, 55}.

2.2.3. Particles Morphology and Synthesis of Superstructures

The presence of foreign molecules and ions also affect the morphology of CaCO_3 particles. The additives can be soluble or insoluble, organic or inorganic solvents, and synthetic or natural polymers^{3-4, 14, 44-45, 55}. Insoluble additives are usually employed as templates to control the nucleation step and influence the crystal growth pattern⁵⁶. In most cases, the additives are co-precipitated with the particles, and can give rise to the formation and growth of superstructures. The literature abounds with studies aimed at the synthesis of CaCO_3 particles with unusual morphologies using additives. Figure 2.3

is a collage of CaCO₃ structures synthesized with different solvents as additives. It was obtained from Boyjoo et al. ⁵⁷.

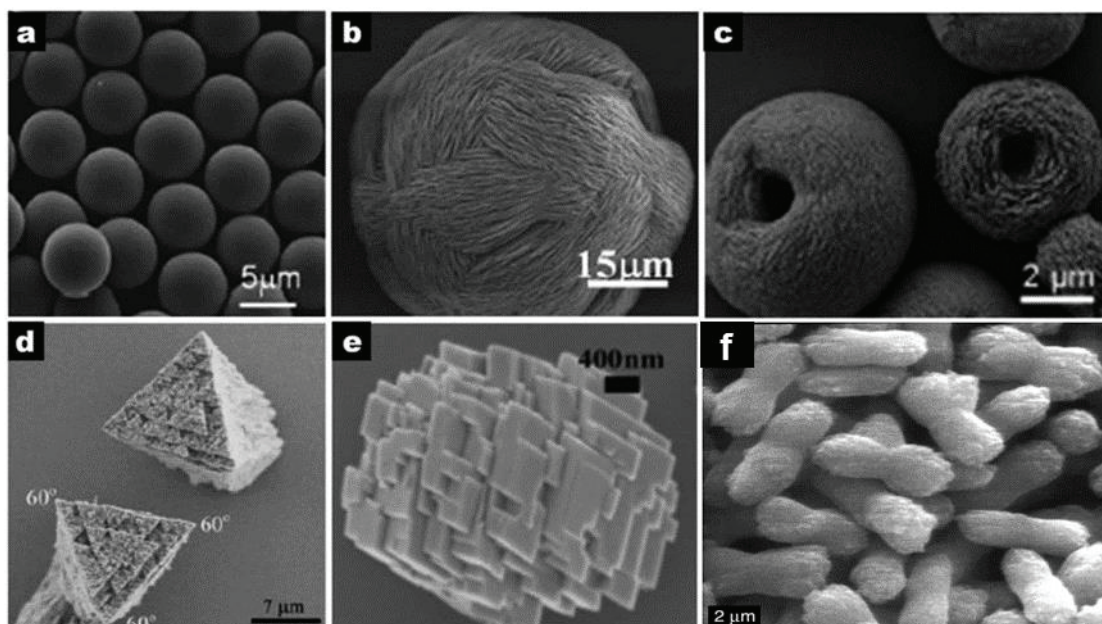


Figure 2.3. Morphosynthesis of CaCO₃ with: (a) *N,N*-dimethylformamide (DMF) ⁵⁸; (b) mixture of *p*-aminobenzene sulfonic acid and L-Lys ⁴⁵; (c) poly(ethylene glycol)-*b*-poly(aspartic acid) ⁵⁹; (d) poly(styrene-*alt*-maleic acid) ⁶⁰; (e) dimethyldioctadecylammonium bromide (DDAB) ⁶¹; (f) poly(ethylene glycol)-*b*-poly(methacrylic acid) ⁶².

2.2.4. Particles Growth Inhibition

Preferential adsorption of ionic species or substances foreign to CaCO₃, on the crystals surface or incorporation within the lattice also effectively retards the overgrowth ^{26, 28, 53, 63}. The mechanism of CaCO₃ growth inhibition by incorporated substances is explained, in previous studies, as an effect of the blockage of growth steps in the crystals lattice and/or dehydration ⁶⁴⁻⁶⁶.

Kontrec et al. ²⁷ investigated the effects of different polysaccharides on the nucleation and growth of CaCO₃ polymorphs. It was reported that non-ionic dextrans not only prevented the crystallization of vaterite in favor of calcite, but also inhibited the overgrowth of calcite. This was evidenced by the reduction in the particles size, which was observed to vary inversely as the molecular weight of the dextran.

Similarly, Jung et al. ⁶⁷ argued that either Ca^{2+} or CO_3^{2-} ions can significantly inhibit the crystals overgrowth and modify the particle morphology, if present in excess quantities in the reaction mixtures. The largest average particles sizes were observed when the reactants were provided in stoichiometric amounts. The authors concluded the growth inhibition was a result of the adsorption of excess ions onto the crystal faces and the consequent blocking of growth sites.

2.3. Chemical Precipitation of CaCO_3 Nanoparticles

CaCO_3 nanoparticles are often obtained in carbonation processes, particularly at the earliest stages. This is due, in large part, to the presence of excess Ca^{2+} ions in the $\text{CO}_2(\text{g})$ absorbing solution ^{4, 67-68}. However, as earlier stated, the synthesis of CaCO_3 nanoparticles in chemical precipitation methods is a rarity, except in very dilute conditions. In the absence of inhibitors, a major factor affecting the particles sizes is the concentration of precipitants – the saturation index.

Wei et al. ¹⁹ prepared ~500 nm hollow vaterite particles for controlled drug release by mixing 2 mM of CaCl_2 and Na_2CO_3 solutions. This is probably the least particles size reported in studies aimed at inhibiting CaCO_3 crystals growth and/or synthesizing them in nano-dimensions, using a chemical precipitation method. In this case, soluble starch was used as a template to control the crystallization process, halting the polymorphic transformation steps and creating microspheres in the particles where the anticancer drugs were encapsulated.

2.4. Electrical Double Layer and ζ -potential Theory

An electrical double layer is said to develop around suspended particles, in response to the charges that exist on the particles surfaces ⁶⁹. The development of net charges on particles affects the distribution of ions at their interfaces with the dispersion medium. This leads to higher concentration of opposite-charge ions in the regions closest to the particles surfaces. As shown in Figure 2.4, the liquid layer of the interface is divided into two parts: the Stern layer, where the counter ions are strongly bound to the particles surface; and a diffuse layer where they are much less attached. The greatest concentration of the counter ions is found in the Stern layer, while progressively lower

concentrations is found at greater distances from the particles surfaces ⁷⁰. There will be a relatively equal distribution of opposite charges in the regions farthest into the solution, resulting in low electrical potential.

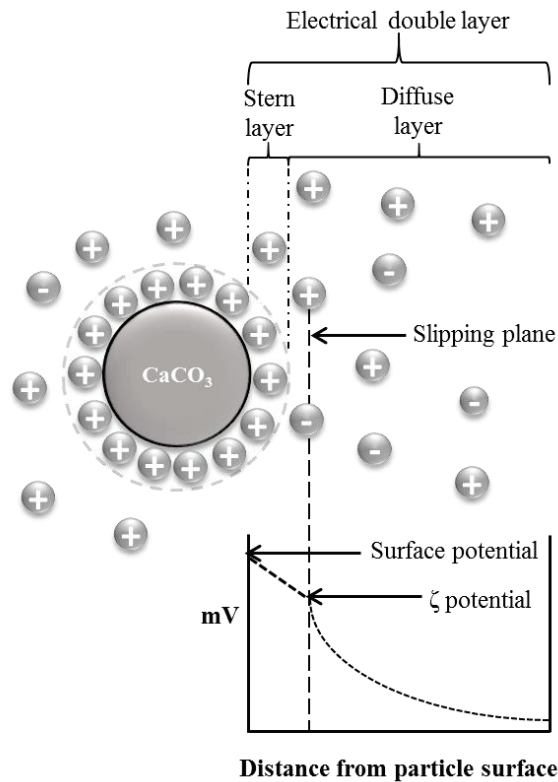


Figure 2.4. Electrical double layer (Source: Malvern ⁷⁰).

There is a boundary inside the diffuse layer, where the particles and ions are acknowledged to form stable entities. The boundary is known as the surface of hydrodynamic shear or slipping plane, and it is based on the no-slip condition frequently applied in modelling fluid flow at solid-liquid interfaces ⁷¹. It states that the liquid layer adjacent to a solid surface assumes the velocity of the surface. By implication, when the particle moves in the solution, ions within this notational boundary move with it.

The electrical potential at the slipping plane is the particles ζ -potential, and it is a measure of its stability in the suspension. The tendency to aggregate is higher when the absolute value of the ζ -potential is low; but particles that possess high ζ -potential, either positive or negative, tend to repel each other. A dispersed phase is usually regarded colloidally stable when the ζ -potential is larger than ± 30 mV ³¹. The suspensions pH is an important factor that affects the ζ -potential. A particle (suspended in pure water) with a positive ζ -potential would acquire more positive charge if more acid is added to the

suspension. If an alkali is gradually added, the pH where the particles ζ -potential is zero will be reached. This is known as the isoelectric point ⁷². In such cases, further addition of alkali can lead to increase in the negative charge accumulated towards the particles surface, and hence, the absolute value of the ζ -potential.

2.5. CaCO₃ Colloidal Stability in Excess Ca²⁺ Ions Conditions

Kilic et al. ³¹ observed that CaCO₃ particles dispersed in Ca(OH)₂ solutions had ζ -potentials greater than +30 mV, which is a benchmark for colloidal stability. CaCO₃ particles surfaces are usually negatively-charged: therefore, a positive ζ -potential indicates the adsorption of Ca²⁺ ions from the Ca(OH)₂ on the particles surfaces. Chibowski et al. ⁷³ made a similar observation, and also showed that excess Ca²⁺ ions adsorbed irreversibly on the particles surface, as the ζ -potential remained unchanged an hour after the precipitation process had completed.

In the light of these observations, the adsorption of excess or additive Ca²⁺ ions on freshly-precipitated particles, obtained from conventional chemical precipitation methods is expected to improve electrostatic repulsion among the crystals, thus reducing their tendency to agglomerate, inhibiting their growth and impeding their sedimentation. CaCO₃ particles produced in chemical precipitation methods at relatively high saturation indexes are usually larger than 3 μm , and no method has been suggested so far, to synthesize nano-sized particles in such cases. Here, it is proposed that nano-CaCO₃ particles can be obtained by the dispersion of fresh precipitates in Ca(OH)₂ solutions.

2.6. Why Ca(OH)₂?

Suitable additives or growth inhibitors should be carefully selected, as their nature can limit the potential application of the synthesized particles. The process of removing toxic or carcinogenic additives can be expensive and their trace amounts will pose a major drawback in the use of such particles in food packaging, cosmetics, pharmaceutical and biomedical applications ⁷. Ca(OH)₂ overcome these limitations for a number of reasons: (1) it is a source of Ca²⁺, an ion known to favor the formation of calcite; (2) it has not been associated with any chronic illness; (3) it is relatively cheap and easy to acquire ^{7, 67, 74}.

CHAPTER 3

EXPERIMENTAL PROCEDURE

3.1. Materials

All reagents were of analytical grade and used without further purification: CaCl_2 (assay $\approx 90\%$, Merck), Na_2CO_3 ($\geq 99.5\%$, Merck), $\text{Ca}(\text{OH})_2$ ($\geq 96\%$, Merck), acetone (CH_3COCH_3 ; assay $\geq 99\%$, Carlo Erba Reagents) and HCl (37% w/w, Sigma-Aldrich). The solutions were prepared in ultrapure deionized water obtained from Milli-Q water purification system (resistivity $\approx 18.2 \text{ M}\Omega\cdot\text{cm}$; Millipore).

3.2. Experimental Setup

The experimental setup is shown in Figure 3.1. In a semi-batch design, Na_2CO_3 and CaCl_2 of equimolar concentrations were each drawn by a peristaltic pump from stock solutions at a constant rate of $7.5 \text{ mL}\cdot\text{min}^{-1}$, and reacted in a model tubular reactor. Thus, in all the experiments, the flowrate of the reaction mixture through the reactor was $15 \text{ mL}\cdot\text{min}^{-1}$.

After contact at the mixing tee, the reaction mixtures containing the precipitated particles were fed into continuously stirred $\text{Ca}(\text{OH})_2$ solutions of known concentrations for particles growth inhibition and stabilization. The suspensions were stirred at 500 RPM and kept airtight throughout the duration of each run. The experiments were carried out under atmospheric pressure and ambient temperature in the range $24\pm 2^\circ\text{C}$.

Unlike co-precipitation techniques, this method separates the crystals nucleation and growth stages. The particles were precipitated in the tubular reactor, which extends from the mixing tee, while the growth inhibition was conducted in a 500 mL vessel having five necks.

CaCO_3 particles were synthesized under free-drift conditions: the suspensions pH and composition were not controlled. As illustrated in Figure 3.1, changes in the suspensions specific conductance and pH were collected online using a Thermo Scientific Orion 5 Star meter fitted with a conductivity probe and glass pH electrode.

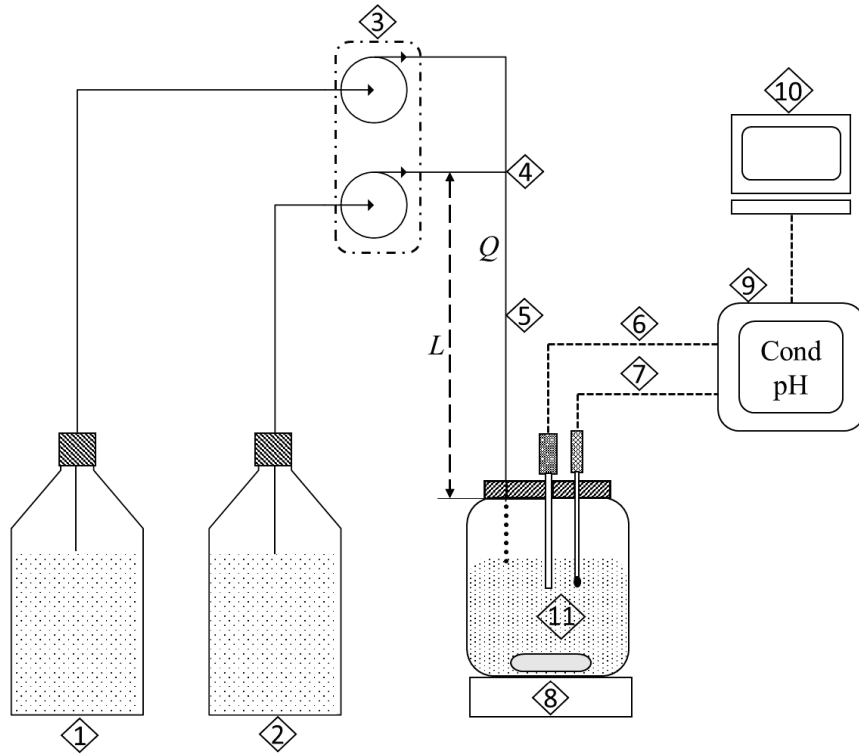


Figure 3.1. Experimental setup: 1. Na_2CO_3 solution; 2. CaCl_2 solution; 3. Peristaltic pump; 4. Mixing tee; 5. Tubular reactor; 6. Conductivity probe; 7. pH probe; 8. Magnetic stirrer; 9. Conductivity and pH meter; 10. Computer; 11. $\text{Ca}(\text{OH})_2$ solution.

3.3. The Tubular Reactor

The particles were precipitated in a silicone tube with 3 mm internal diameter (d), before dispersion into the stabilizing and growth-inhibiting $\text{Ca}(\text{OH})_2$ solution. With a total volumetric flowrate (Q) of $15 \text{ mL} \cdot \text{min}^{-1}$, the stream velocity was calculated as $\sim 212 \text{ cm} \cdot \text{min}^{-1}$ using Eq. 3.1. At 25°C and atmospheric pressure, the dynamic viscosity (μ) and density of water (ρ) are $8.91 \times 10^{-4} \text{ Pa} \cdot \text{s}$ and $997.13 \text{ kg} \cdot \text{m}^{-3}$, respectively. By assuming the solutes or particles concentration in the reactor does not significantly affect the fluids density and viscosity, the Reynolds number (Re) was calculated to be ~ 119 , using Eq. 3.2. The Reynolds number indicates a laminar flow regime in the model tubular reactor.

$$v = \frac{4Q}{\pi d^2} \quad (3.1)$$

$$Re = \frac{dv\rho}{\mu} \quad (3.2)$$

The tubular reactor was either changed for each run or washed by pumping a dilute acid solution and ultrapure H₂O through the tubing, so as to avoid errors that could result from the presence of CaCO₃ precipitates formed on the inner walls from a previous experiment.

3.4. Studied Parameters

A summary of the studied parameters is presented in Table 3.1. The effects of these parameters on the particles size, colloidal stability (ζ -potential), morphology, specific surface area and crystal form were investigated. In a particular case, time-dependent changes in the aforementioned particle properties were examined.

Table 3.1. Studied experimental parameters.

Parameter	Range
Residence time (τ)	1 sec. – 2 min.
Precipitants concentration (C_A)	25 – 100 mM
Ca(OH) ₂ concentration (C_S)	0 – 15 mM
Precipitants volume	50 – 400 mL
Solutions initial pH	9 – 12.5

3.4.1. Residence Time

A major limitation in the study of CaCO₃ systems is the rate at which it precipitates, crystallizes and grows. Studies that discuss its polymorphic transformation and growth mechanisms are usually conducted under conditions designed to delay the reactive crystallization step or capture the occurring changes on a timescale of seconds^{6, 9, 35, 40, 75-76}. Consequently, the residence time (τ) of the reaction mixtures in the tubular reactor was varied by adjusting the reactor length (L). It was calculated with Eq. 3.3, using the total volumetric flowrate (Q).

$$\tau = \frac{L}{Q} \cdot \frac{\pi d^2}{4} \quad (3.3)$$

It was presumed that the retention of the precipitates in the tubular reactor longer than might be necessary, might afford the crystals more time to grow and aggregate before reaching the stabilizing solution, thereby reducing the additive Ca^{2+} ions inhibitory efficiency. In each studied case, the objective was to examine the effects of the residence time on the particles size and colloidal stability. The precipitants concentration (C_A) was varied between 25 – 100 mM, and the precipitates were continuously dispersed in 250 mL of 10 mM $\text{Ca}(\text{OH})_2$ solution. 1 mL samples were taken from the stabilizing solution each minute, up to the 8th minute. Here, only the particles hydrodynamic size and ζ -potential were measured.

3.4.2. Time-dependent Changes in Particle Properties

Particle growth and evolution of the morphology, crystal nature and specific surface area during the growth inhibition process was studied for $C_A = 75$ mM and $\tau = 2$ minutes, a condition where vaterite could have crystallized in the tubular reactor⁶. With $\tau = 2$ minutes, another objective was to determine the possible effects of the formation of crystalline CaCO_3 in the tubular reactor. The precipitates were stabilized in 250 mL of 10 mM $\text{Ca}(\text{OH})_2$, and the entire suspension was centrifuged at the end of each minute, in order to obtain sufficient particles for characterization. Also, keeping all other variables constant, a control experiment was conducted using ultrapure DI H_2O as the growth-inhibiting solution and the particles were collected at the 8th minute.

Kilic et al.³¹ reported that the conductivity of $\text{Ca}(\text{OH})_2$ solution varies linearly as the molar concentration, up to ~20 mM. However, Na^+ and Cl^- are counter ions of the precipitants used in this study. Their presence results in ionic interactions that alter the suspensions conductivity. This necessitates the use of a different method to experimentally determine changes in Ca^{2+} ions concentration in the growth-inhibiting solution. Therefore, ion chromatography was carried out with a Thermo Scientific Dionex ICS 5000+ equipped with a conductivity detector, to measure the concentration of both Ca^{2+} and Na^+ ions in the suspension per time. Samples were taken each minute from the solution, and the suspended CaCO_3 particles were separated with a 0.22 μm

filter. The mobile phase in the chromatograph was 30 mM methanesulfonic acid with a flowrate of 1 mL·min⁻¹.

3.4.3. Additive Ca²⁺ ion and Precipitants Concentration

Transformation of amorphous CaCO₃ (ACC) to any CaCO₃ polymorph proceeds rapidly after precipitation^{6, 9, 40, 76}. According to Bots et al.⁶, vaterite polymorph, which is a precursor phase for the precipitation of calcite at room temperature, appears after ~70 seconds under conditions of high supersaturation. For this reason, the residence time of the reaction mixtures was kept low, such that only ACC would precipitate in the reactor. Here, predefined volumes of the precipitants were reacted with $\tau = 9$ seconds, and the precipitates were continuously dispersed in 200 mL of Ca(OH)₂ solutions. The time required to deliver the desired amounts was calculated from the flowrate. For instance, in 400 seconds, 50 mL of each reactant would have been pumped through the reactor.

Effects of the Ca(OH)₂ solutions initial concentration could only be assessed up to 15 mM, due to its limited solubility in water which was found in an earlier study to be ~18 mM at 23°C³¹. The volume and concentration of the precipitants were varied from 50 to 400 mL and 25 to 75 mM, respectively. For comparison purposes, some control studies were completed using ultrapure DI H₂O in place of Ca(OH)₂ solution. The influence of the reactants volume and concentration, and Ca(OH)₂ concentration on the particles size, morphology, ζ -potential, polymorphic form, and specific surface area were studied.

3.4.4. Growth-inhibiting Solutions initial pH

The purpose here was to determine the probable pH effects on the growth inhibition process. Though the stabilizing solutions initial pH was varied, the process was still allowed to proceed spontaneously. 50 mL of precipitants with $C_A = 25$ mM were reacted in the tubular reactor. The precipitated particles stabilization and growth inhibition were attempted in 200 mL of 10 mM Ca(OH)₂ solution. The solutions initial pH was adjusted with 5 M HCl in order to eliminate possible volume change effects. Also, the conductivity and pH changes were collected online.

In a separate experiment, NaOH was used in place of Ca(OH)₂. The objective was to further understand the role of additive Ca²⁺ ions and high alkaline conditions on the particles properties. 200 mL of NaOH solution with pH ≈ 13 was prepared by dissolving ~0.25 g of NaOH crystals in H₂O. The particles size, colloidal stability and morphology were compared with those obtained when H₂O and Ca(OH)₂ solution were used as the particles stabilizing and growth-inhibiting solution.

3.5. Particle Characterization

In all the experiments, dynamic light scattering (DLS) method with Zetasizer Nano-ZS (ZEN3600, Malvern) was used to determine the particle size and distribution. It assumes a spherical shape for the particles and measures the mean hydrodynamic diameter^{24, 34, 77}. In cases where it was possible, the Zetasizer was also used to determine the ζ-potential of the dispersed phase. Particles with sizes larger than ~4 μm were generally observed to be rapidly settling, and considered not suitable for DLS method. In such situations, a Coulter Counter (Multisizer 4, Beckman Coulter) fitted with a 30 μm aperture which allows for size measurements up to 18 μm was used instead.

In experiments where powder samples were collected and characterized, the suspensions were centrifuged, washed with pure acetone and dried *in vacuo* at 85°C for 24 hours. Samples were gold coated and imaged on a Carl Zeiss 300VP scanning electron microscope (SEM). X-ray diffraction (XRD) data were obtained from a PANalytical Empyrean diffractometer using Cu-K_α radiation. The 2θ scan range, step size and K_{α1}/K_{α2} are 10 to 80°, 0.013° and 0.5, respectively. Rietveld refinement was carried out on the diffraction data using X'Pert Highscore Plus software, to determine the relative abundance of each polymorph in the samples. At ambient temperature (~25°C), a Micromeritics Gemini V Surface Area Analyzer was used to assess the particles specific surface area (SSA) with Brunauer–Emmett–Teller (BET) method using N_{2(g)}. The degassing was conducted at 105°C.

CHAPTER 4

RESULTS AND DISCUSSION

In this thesis, C_A and C_S are the precipitants and starting $\text{Ca}(\text{OH})_2$ solutions concentration, respectively.

4.1. Residence Time Effects

Here, the particles retention time in the tubular reactor was varied by changing the reactor's length, and samples were taken from the stabilizing solution each minute for hydrodynamic size and ζ -potential measurements. The size and ζ -potential of particles initially present in the starting $\text{Ca}(\text{OH})_2$ solution were also measured. Changes in the hydrodynamic diameter of the particles and ζ -potential at different values of τ and C_A , with respect to time, are presented in Figure 4.1 and Figure 4.2 respectively. The initial mean size of suspected CaCO_3 particles in the $\text{Ca}(\text{OH})_2$ solution was ~ 300 nm, which is attributable to its presence as an impurity constituting $\sim 3\%$ of the acquired $\text{Ca}(\text{OH})_2$ powder.

The amount of CaCO_3 precipitated is a function of the process duration. For all τ , the sizes of the particles in the growth-inhibiting solution increased as more precipitates were dispersed. While the retention of the precipitates in the tubular reactor for a shorter time was expected to yield smaller particles, the particles were generally of the same measure, irrespective of τ , particularly when $C_A \leq 75$ mM.

Larger particles were obtained at higher C_A (Figure 4.3) due to higher concentration of the lattice ions, which results in increased crystals initial growth rate and size²⁶. Figure 4.1a shows the particles were relatively smaller when $C_A = 25$ mM and $\tau = 9$ seconds. Nonetheless, the variations at other residence times, can be considered insignificant since the particles sizes, at all times, do not exceed 130% of the corresponding values at $\tau = 9$ seconds. When $C_A = 100$ mM, the hydrodynamic sizes at $\tau = 1$ second were significantly larger than the values obtained when $\tau = 9$ seconds (Figure 4.1d). The difference in the sizes in these two cases was observed to be initially increasing, with a maximum of ~ 2 μm in the 3rd minute.

Besides growing, the particles also undergo polymorphic transformations: amorphous CaCO_3 is an unstable phase and a precursor to crystalline CaCO_3 ^{6, 9, 39-40, 75}. Under high supersaturation conditions, at room temperature and in presence of no impurity ions or additives, Bots et al.⁶ showed that the first vaterite particles appear after ~ 70 seconds. From Figure 4.1c, when $\tau = 2$ minutes, a case where vaterite would have crystallized in the tubular reactor, the particles hydrodynamic sizes do not significantly differ from the values obtained when $\tau = 1$ second, a condition where only the amorphous phase presumably reaches the stabilizing solution. Thus, the particles size can be said to be largely unaffected by the occurrence of crystalline CaCO_3 in the tubular reactor.

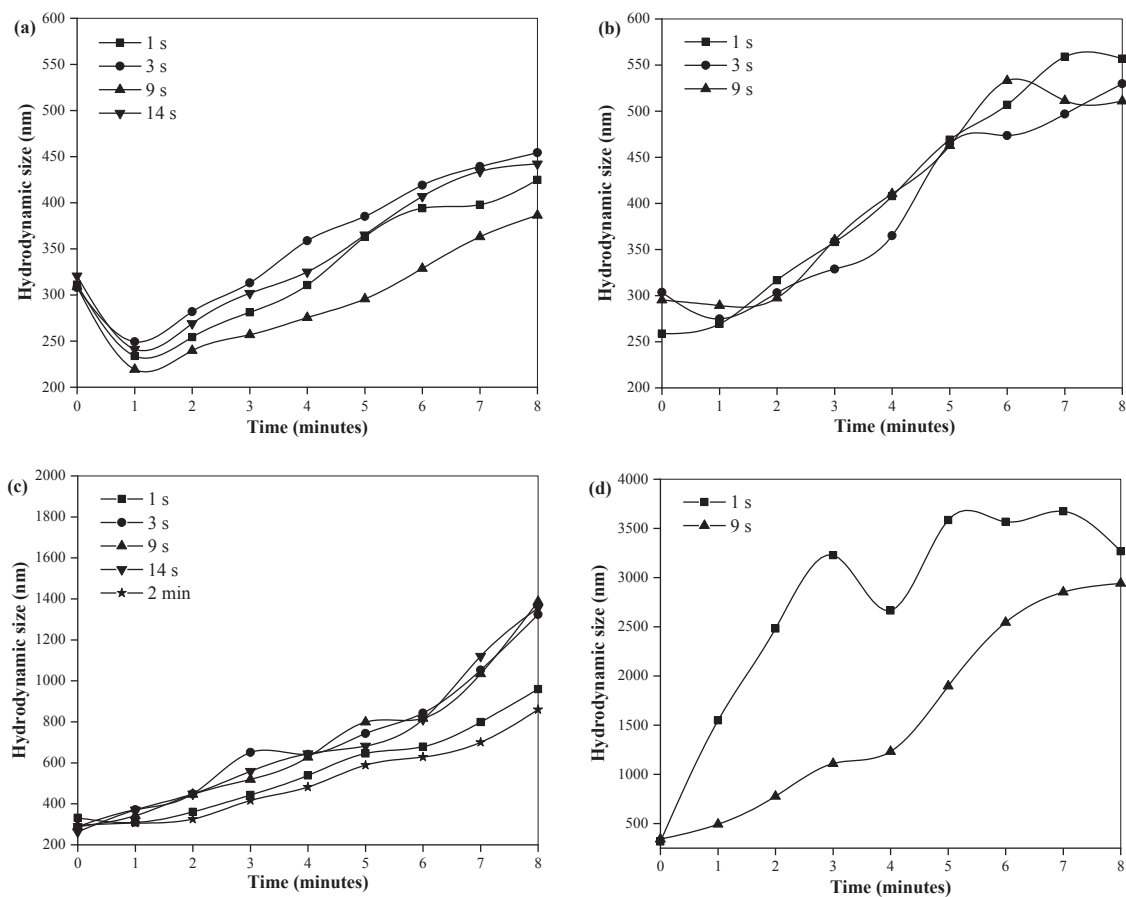


Figure 4.1. Particles size change during stabilization in 250 mL of 10 mM Ca(OH)_2 solution: $C_A =$ (a) 25 mM; (b) 50 mM; (c) 75 mM; and (d) 100 mM.

Suspended particles are considered most stable when their ζ -potential is well above ± 30 mV^{4, 31}. The trend when $C_A = 100$ mM (Figure 4.2d) shows the ζ -potential decreased for both $\tau = 1$ and 9 seconds cases. The dispersed particles also sedimented

rapidly, upon the expiration of the experiments duration. This is due to higher supersaturation and consequent precipitation of larger particles^{9, 26, 41}.

On the other hand, the ζ -potential data at $C_A < 100$ mM is quite difficult to interpret, much more in terms of the effects of the residence time⁷². Nevertheless, as shown in Figure 4.2, it was positive in all the cases studied. This demonstrates the adsorption of the additive Ca^{2+} ions on the particles surface as both synthetic and naturally occurring CaCO_3 crystals – without the contamination of foreign cations or presence of excess Ca^{2+} ions – are known to possess negatively-charged surfaces^{31, 72-73, 78}.

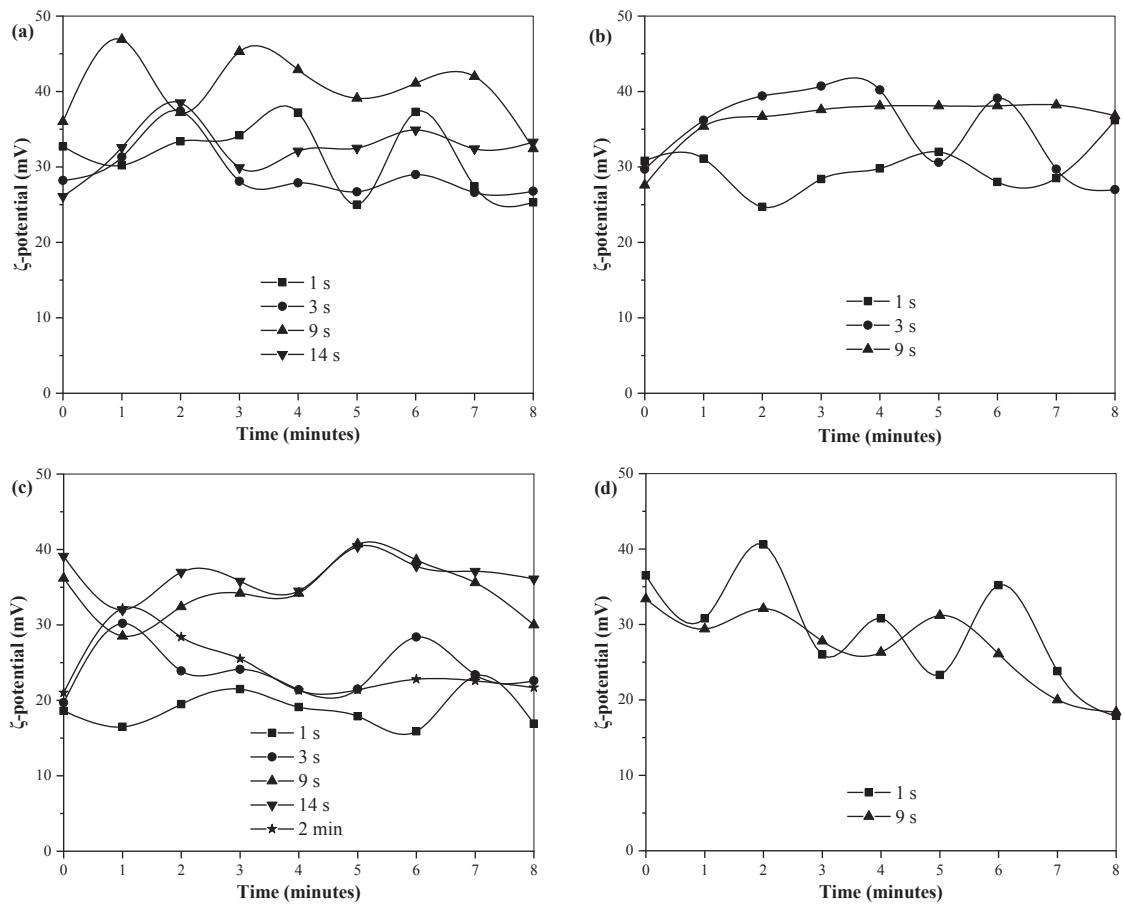


Figure 4.2. ζ -potential change during stabilization in 250 mL of 10 mM $\text{Ca}(\text{OH})_2$ solution: $C_A =$ (a) 25 mM; (b) 50 mM; (c) 75 mM; and (d) 100 mM.

For $C_A = 75$ mM case, there is a significant difference between the hydrodynamic sizes of the particles at the 8th minute when $\tau = 9$ seconds and $\tau = 2$ minutes (Figure 4.1c). It was $\sim 1.4 \mu\text{m}$ at $\tau = 9$ seconds and ~ 850 nm when $\tau = 2$ minutes. At longer times, the particles ζ -potential at $\tau = 9$ seconds was higher than that obtained at $\tau = 2$ minutes.

This suggests there is a probable trade-off between particle size and stability, based on the choice of τ . Moreover, Figure 4.2a-c show the particles at $\tau = 9$ seconds were more stable in the suspension (≈ 30 mV) compared to those at other values of τ examined. It suggests if the precipitants are allowed enough time to react, on a scale of seconds, relatively small and stable particles can be obtained from the growth-inhibiting solution. Figure 4.3 confirms the possibility of synthesizing stable CaCO_3 nanoparticles when $C_A \leq 75$ mM.

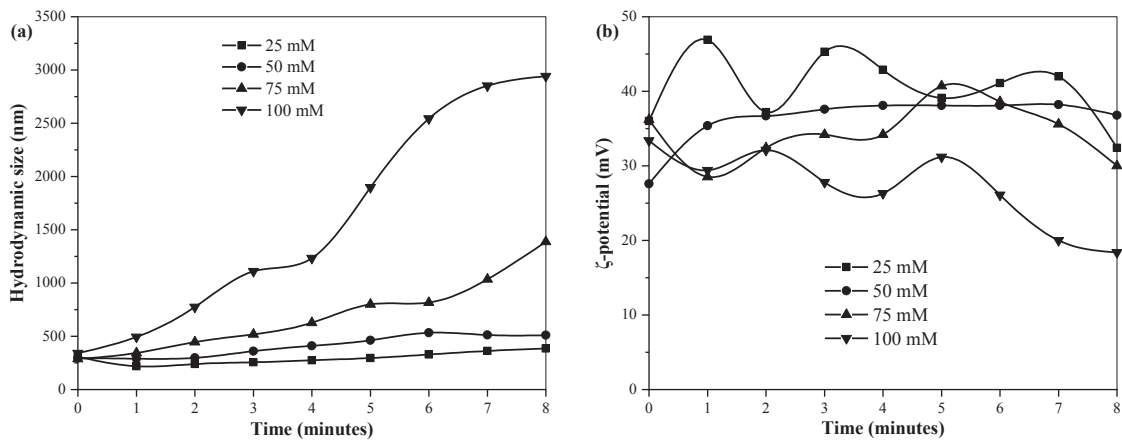


Figure 4.3. Particles stabilization in 250 mL of 10 mM Ca(OH)_2 solution. Effects of C_A on (a) particles size and (b) ζ -potential, when $\tau = 9$ seconds.

4.2. Evolution of Particle Properties

With $C_A = 75$ mM and $\tau = 2$ minutes, time-dependent changes in the particles morphology, specific surface area (SSA) and crystal form during the growth inhibition process were studied. The precipitates were dispersed in 250 mL of 10 mM Ca(OH)_2 solution.

The particles size were observed to only increase as more precipitates reached the growth-inhibiting solution. As shown in Figure 4.4, the mean size was ~ 300 nm in the 1st minute, steadily increased, reaching ~ 850 nm in 8th minute. This growth is also evident in the size distribution analyses (Figure 4.5). The distribution curve of the initial state does confirm the Ca(OH)_2 solution contained particles considerably larger than $1 \mu\text{m}$, which are presumed to be CaCO_3 particles present as impurities in the Ca(OH)_2 powder.

The size distribution curves shifted to the right, indicating increase in the mean particle size per time. Nonetheless, they remained monomodal. Their widths are relatively small and do not indicate the presence of large amounts of large particles or aggregates in the suspension. The distributions at the 6th, 7th and 8th minutes lie in the same domain, and more than 60% of the samples were particles with sizes between ~400 and ~600 nm. However, the mean sizes vary quite significantly, increasing from ~600 nm in the 6th minute to ~850 nm in the 8th. This is due to the presence of slightly more large particles in the sample in the 8th minute. Since additive Ca^{2+} ions adsorb irreversibly on the earliest particles, the amount available as growth inhibitors reduces as more precipitate is fed into the solution. Moreover, the presence of few large particles or agglomerates in a sample can undesirably impact the precision of DLS method.

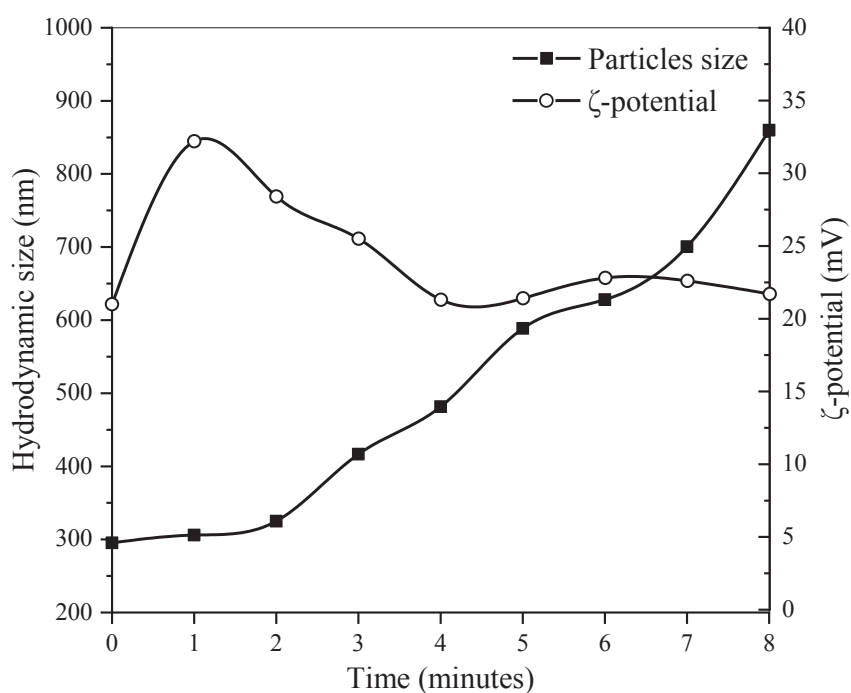


Figure 4.4. Time-dependent changes in size and ζ -potential of particles stabilized when $C_A = 75$ mM and $\tau = 2$ minutes.

The presence of additive Ca^{2+} ions also effected the particles colloidal stability. The ζ -potential data (Figure 4.4) indicates the particles were most stable in the 1st minute. This was expected as there are more free additive Ca^{2+} ions at the start of the process. The ζ -potential reduced with increasing volume of particles in the suspension, but remained somewhat constant beyond the 4th minute. The particles were still fairly colloidal stable in the 8th minute, with a ζ -potential of ~22 mV. In any case, if more

particles are precipitated, the depletion of the additive Ca^{2+} ions by irreversible adsorption on the first crystals will eventually cause the solution to lose its growth inhibitory efficiency, and result in further particle growth and agglomeration^{26,41}. Thus, synthesizing more stable nanoparticles will necessitate a higher concentration of free Ca^{2+} ions^{26,65}.

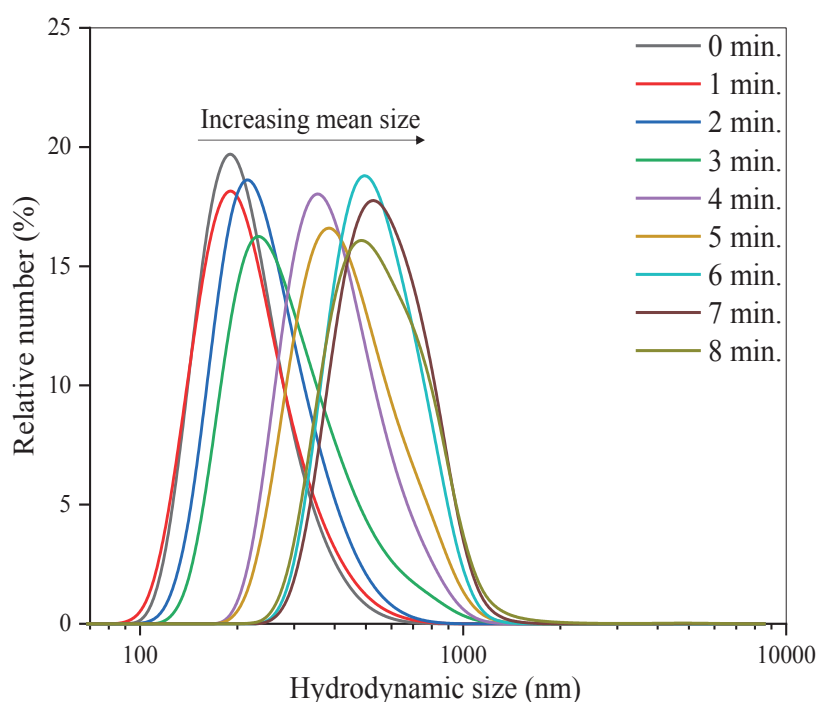


Figure 4.5. Time-dependent changes in particles size distribution when $C_A = 75$ mM and $\tau = 2$ minutes.

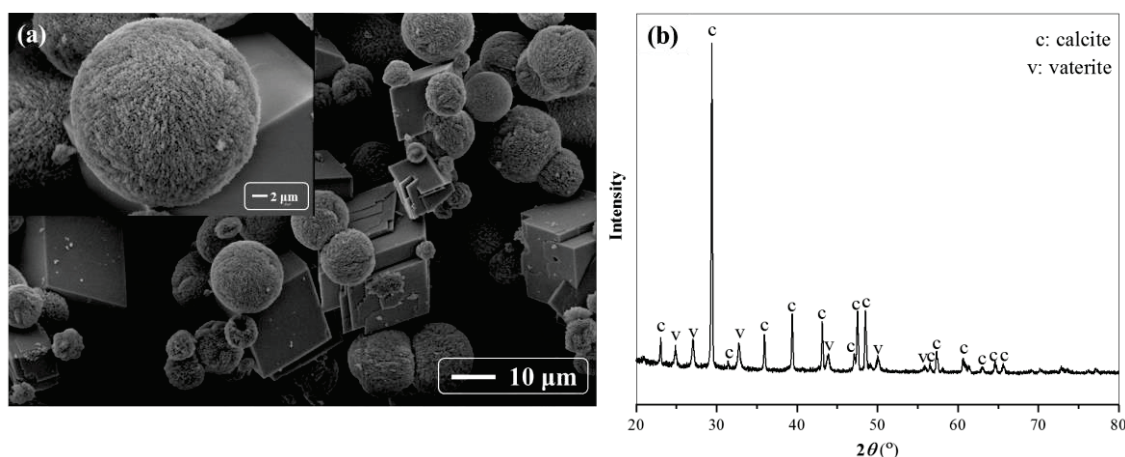


Figure 4.6. Properties of particles stabilized in ultrapure DI H_2O at the 8th minute when $C_A = 75$ mM and $\tau = 2$ minutes: (a) XRD pattern; (b) Morphology and polycrystalline vaterite (inset in b).

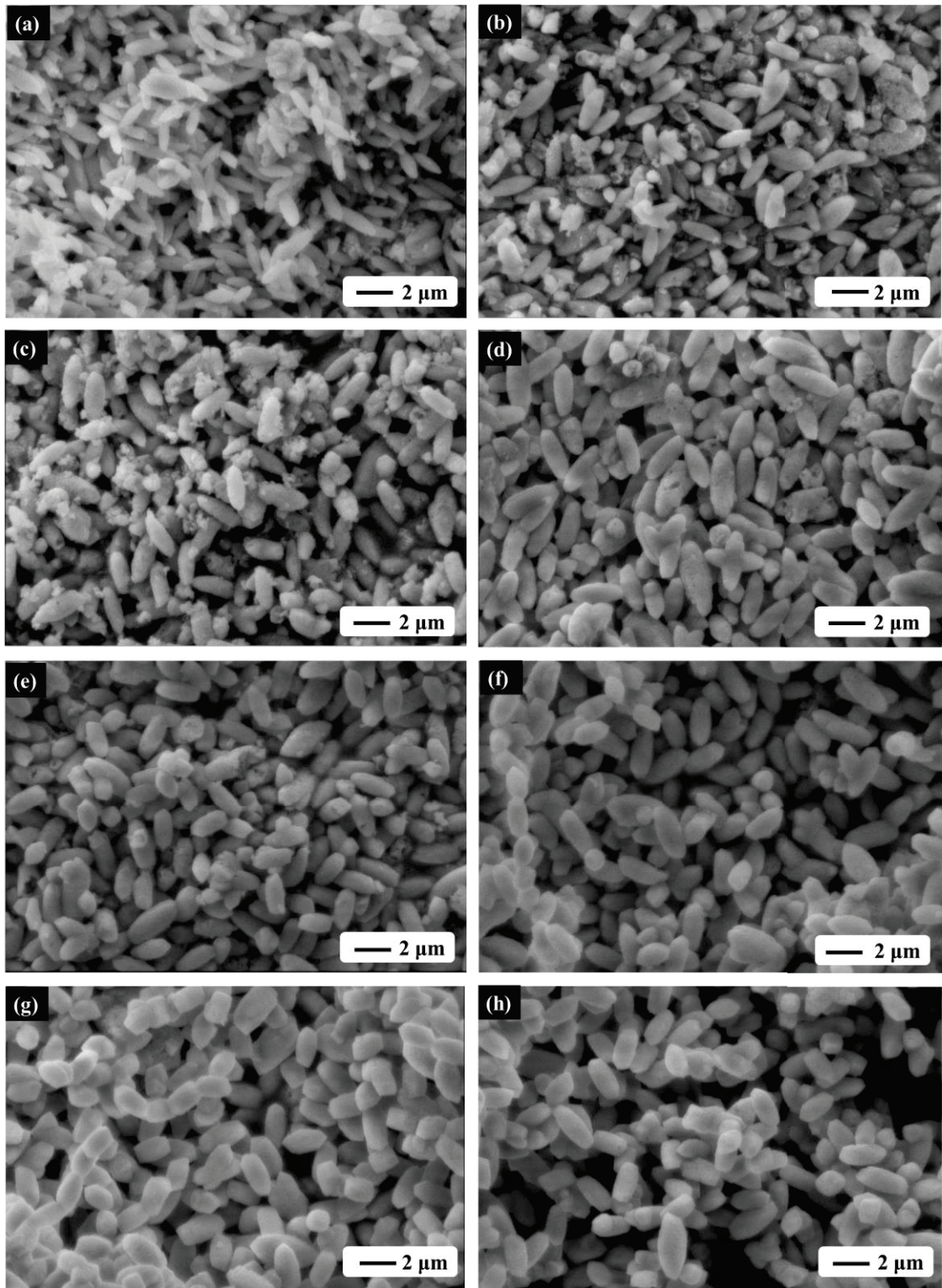


Figure 4.7. Time-dependent particles morphology changes when $C_A = 75$ mM and $\tau = 2$ minutes: (a) – (h), 1st – 8th minute respectively.

On the other hand, the hydrodynamic size of the particles obtained in the 8th minute, after attempting stabilization and growth inhibition in H_2O , could not be

determined with DLS method. The particles were unstable in the suspension and rapidly settled after the experiment. This is because, to attain equilibrium, crystals must possess the lowest possible surface free energy per unit volume. Since surfaces with high free energies have high growth rates, in order to lower their interfacial area to the solution and speedily establish equilibrium, such crystals will grow and agglomerate until a size that engenders sedimentation is reached^{26, 79}. The SEM micrograph (Figure 4.6a) of particles obtained when pure H₂O was used reveals a case of immense aggregation. It can be inferred that the sample might contain ~10 µm-sized individual particles, which is ~12 times the mean hydrodynamic size obtained after growth inhibition in the presence of additive Ca²⁺ ions.

Contrary to the observation in pure H₂O, Figure 4.7 shows the particles synthesized in the presence of additive Ca²⁺ ions were small and somewhat monodisperse. Also, much difference is not observed in the particles dimensions at the 6th minute and beyond: the particles were generally of the same size in this time range. This corroborates the result obtained in the hydrodynamic size distribution analyses (Figure 4.5), which show that majority of the particles from the 6th to the 8th minute were between 400 – 600 nm.

Figure 4.7 also reveals the particles morphology changed as the process progressed. The presence of minuscule rhombohedra and truncated cubes is observable starting from 2nd minute, but the particles were monodisperse spindle-like scalenohedra in the 1st minute. This is consistent with the understanding that scalenohedral calcite crystallizes in excess Ca²⁺ ions conditions^{3-4, 68}. In carbonation methods, scalenohedra transforms into rhombohedra through a dissolution-recrystallization process initiated by the decrease in pH as more CO_{2(g)} dissolves⁴. However, in the current study, the final suspensions pH was greater than 12. Therefore, the gradual morphology changes can be explained as a consequence of the inevitable growth and disruption of the scalenohedral crystals as the volume of suspended particles increased.

As illustrated in the XRD pattern (Figure 4.6b), particles obtained at the 8th minute in the absence of additive Ca²⁺ ions contained both vaterite and calcite phases. Figure 4.6a shows the powder was a mixture of rhombohedra and spheres. Also, Figure 4.6a (inset) indicates the spherical particles are polycrystalline, which is a property of vaterite polymorph and confirms its occurrence as highlighted in the diffractogram. Rietveld refinement revealed the sample was ~34 % vaterite.

Based on Ostwald's rule of stages, since calcite is the most thermodynamically stable polymorph of CaCO_3 , all the vaterite particles observed in Figure 4.6 will eventually be converted into calcite, if sufficient ageing time is allowed. However, they were totally transformed into calcite in the 1st minute, when additive Ca^{2+} ions were present in the suspension (Figure 4.8). This agrees with previous studies which show that excess Ca^{2+} ions influence the conversion of amorphous CaCO_3 into calcite without a metastable intermediate^{1, 3, 55}.

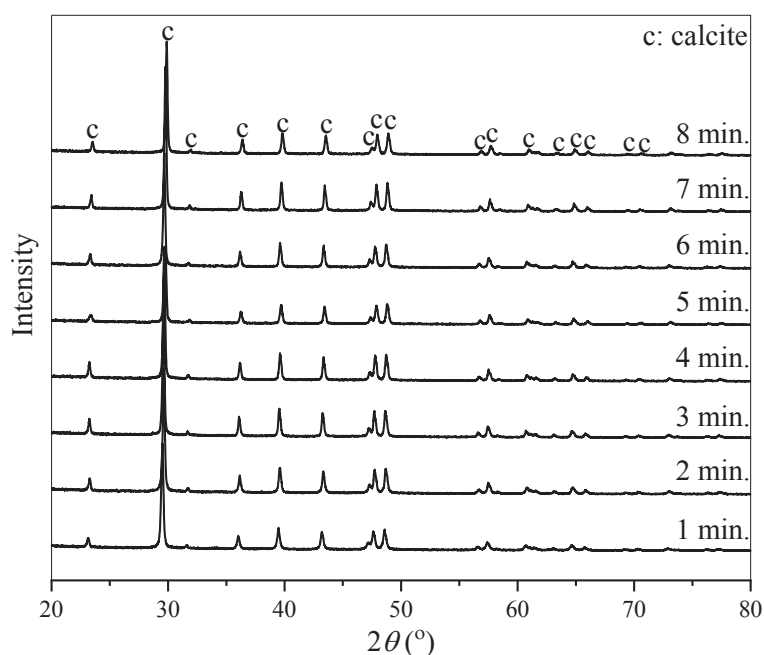


Figure 4.8. Particles Crystal form when $C_A = 75$ mM and $\tau = 2$ minutes.

From Figure 4.7, the erosion of the particles exposed surfaces is intense between the 1st and 5th minute. Pores and pits are apparent in the particles at the beginning, but they diminished with time. This is supported by results obtained from surface area analyses which indicate the presence of pores in the particles. From the 1st minute to the 8th, the average pore size was ~ 5 nm. Figure 4.9a shows the BET particle SSA was highest in the 1st minute, reduced up to the 5th minute, and remained fairly constant afterwards. This implies the pore structures were concurrently filled as the particles grew with more precipitates reaching the solution. The $\text{N}_{2(g)}$ adsorption-desorption isotherm shown in Figure 4.9b also demonstrates the presence of pores in the synthesized particles.

Cavities and pits observed in calcite particles have been reported, based on Ostwald's rule of stages, as an outcome of the crystallization and growth of calcite on

the rough surfaces of a dissolving metastable polymorph⁴⁹. Although the crystallization of vaterite was expected in the tubular reactor at $\tau = 2$ minutes; it is considered too short a period for a spontaneous conversion into a pure calcite phase in the 1st minute. Moreover, vaterite particles were still observed in the powder obtained at the 8th minute in the H₂O case (Figure 4.6).

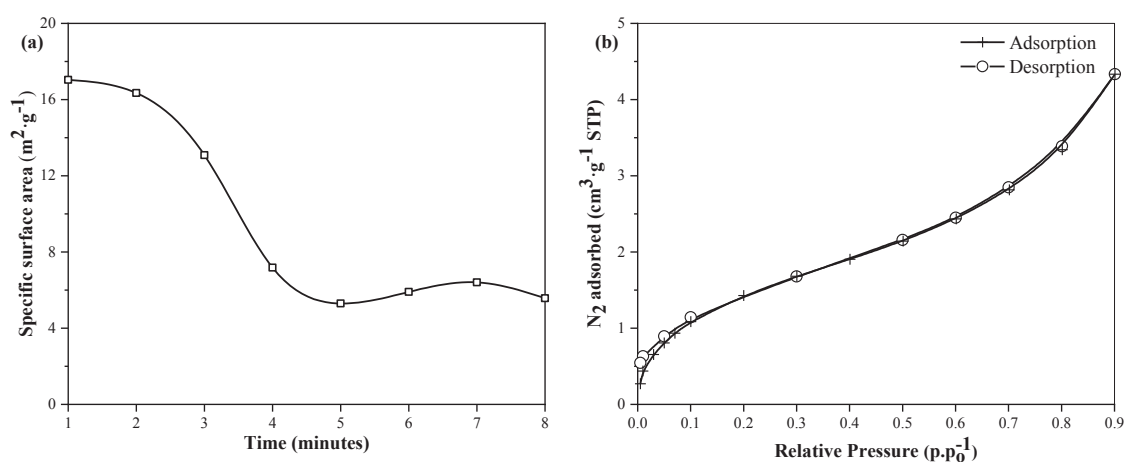


Figure 4.9. Particles surface area analyses for $C_A = 75$ mM and $\tau = 2$ minutes: (a) Time-dependent change in BET SSA; (b) Isotherm linear plot of particles obtained at the 8th minute.

In addition to calcites low solubility product and thermodynamic stability, the suspension will always be saturated with calcite in the presence of additive Ca²⁺ ions, and thus, could not have been dissolving, particularly at pH >12. Moreover, the binding tendency of Ca²⁺ and CO₃²⁻ ions is high in high alkaline conditions³⁶. Therefore, the occurrence of pores in the particles can be regarded as an additional influence of the excess Ca²⁺ ions. This phenomenon is explained as an effect of the particles morphology and crystal form changes, which simultaneously occurred during the growth inhibition process, or absolute poisoning of certain growth sites or steps in the crystals.

Owing to the polar nature of scalenohedral faces, Cizer et al.³ argued that excess OH⁻ ions can also preferentially adsorb on the crystals and, hence, contribute to the retardation of other growth morphologies. However, the inhibition of freshly-precipitated CaCO₃ growth in Ca(OH)₂ solution, as discussed in this study, cannot be interpreted as solely those of a high pH condition. The literature is replete with studies on the effects of pH in CaCO₃ systems, but none has reported the synthesis of submicron CaCO₃

particles, using the chemical precipitation method, except at much lower reactants concentration or degrees of supersaturation¹⁹.

Using the diffractograms (Figure 4.8), Scherrer equation (Eq. 4.1) was applied to estimate the size of the crystallites.

$$D = \frac{K \cdot \lambda}{\beta \cdot \cos\theta} \quad (4.1)$$

Where K is the shape factor (usually taken as 0.9), λ is wavelength of the X-ray source (~ 0.154 nm for Cu- K_{α} radiation), β is the full width at half maximum (FWHM, in radians), and θ is the Bragg angle in radians. Crystallites sizes at the seven definite peaks between 20 and $50 2\theta^{\circ}$ were calculated. The average for each time interval is reported in Figure 4.10. The results show the crystallites grew from ~ 28 nm at the first minute to ~ 36 nm in the third minute, and no significant change is observable afterwards.

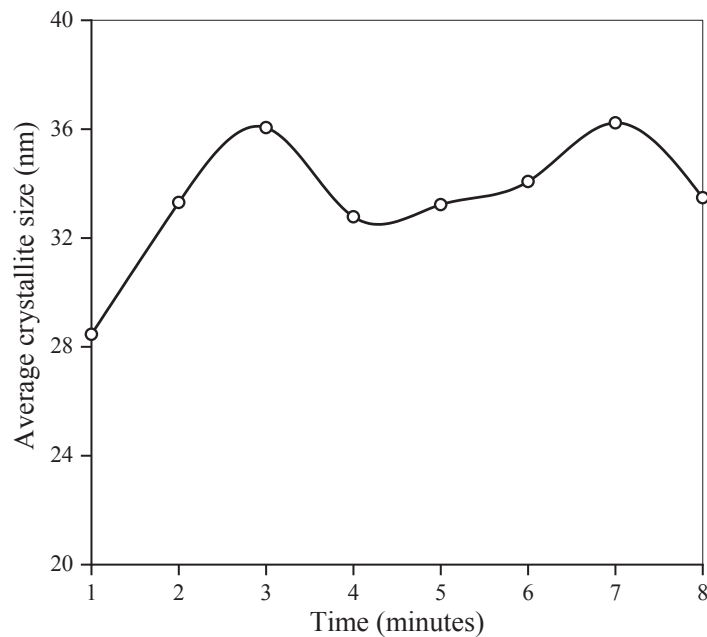


Figure 4.10. Time-dependent changes in crystallites average size when $C_A = 75$ mM and $\tau = 2$ minutes.

Figure 4.4 shows the hydrodynamic mean size of the particles at the 8th minute was ~ 850 nm, which is much larger than the calculated crystallite sizes (~ 33 nm). Since the XRD data and Rietveld refinement analyses indicate the samples were pure calcite particles, a possible explanation for this discrepancy is that the particles are not distinct

or single crystals. Rather, they are agglomerates of much smaller crystallites. This equally makes a case for their porosity, as the aggregation process could have created an open pore structure in the particles.

4.3. Reaction(s) in the Growth-inhibiting Solution?

The continuation of the precipitation reaction in the stabilizing solution is undesirable as it may contribute to crystal growth⁴⁰. Since the purpose is to impede particle overgrowth, it was necessary to ascertain significant chemical reactions were not also occurring in the growth inhibition region. Therefore, the suspensions were left to age for 3 hours, after which samples were again taken for size and ζ -potential measurements. For $\tau = 9$ seconds case, the particles hydrodynamic sizes and ζ -potentials measured at the 8th minute and 3rd hour is presented in Table 4.1. A comparison of the values show the particles did not grow nor agglomerate within the set ageing period. This does not suggest the continuance of reactions in stabilizing solution, which would have resulted in further particle growth. It shows the particles only grew as more precipitates were fed into the suspension.

Table 4.1. ζ -potential and particle size after stabilization and ageing when $\tau = 9$ seconds.

C_A (mM)	8 minutes		3 hours	
	Size (nm)	ζ -potential (mV)	Size (nm)	ζ -potential (mV)
25	386.4	32.4	390.2	39.8
50	510.9	36.8	550.9	35
75	1387	30	1025	25.4
100	2942	18.4	3327	

Figure 4.11 illustrates the conductivity changes for $C_A = 75$ mM and $\tau = 2$ minutes case, when ultrapure DI H₂O and 10 mM Ca(OH)₂ were used for particles growth inhibition. In the ultrapure H₂O case, increase in conductivity is due to the presence of Na⁺ and Cl⁻ ions, which are byproducts of the reaction considered in this study (Eq. 4.2). At the 8th minute, 60 mL of each precipitant would have reacted in the tubular reactor. When $C_A = 75$ mM, 60 mL of CaCl₂ solution is equivalent to 4.5 mmol. With respect to

the reactions stoichiometry, complete reaction or dissolution of the precipitants would produce 9 mmol of Na^+ and Cl^- ions with a concentration of ~ 24.3 mM in the final suspension. This corresponds to a conductivity of ~ 2.75 $\text{mS}\cdot\text{cm}^{-1}$ of NaCl solution, which is the same as the suspensions at the 8th minute. Figure 4.11 shows the conductivity steadily increased to ~ 2.75 $\text{mS}\cdot\text{cm}^{-1}$ when no additive Ca^{2+} ions were in the solution.

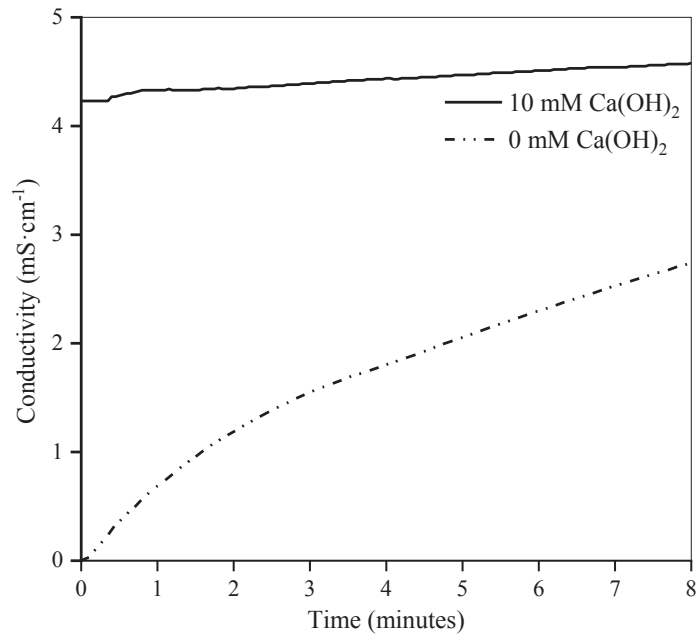


Figure 4.11. Conductivity changes during the growth inhibition process when $C_A = 75$ mM and $\tau = 2$ minutes.



When 10 mM $\text{Ca}(\text{OH})_2$ solution was used for growth inhibition, the conductivity of the suspension remained fairly constant throughout the process. This does not indicate significant reaction(s) between the ionic species, which would have otherwise caused the consumption of more Ca^{2+} ions in the suspension. Reactions involving Ca^{2+} ions would have considerably lowered the conductivity as CaCO_3 is sparingly soluble, especially in high alkaline conditions, and could not have therefore dissociated into its constituent ions in substantial amounts^{1, 4, 8, 80}.

Since the conductivity of a solution is a function of the concentration of ions, as more reaction mixture reaches the stabilizing solution, increase in volume would cause a decrease in the molarity of Ca^{2+} ion in the suspension. This would have resulted in the

reduction of the suspensions conductivity. However, the fairly constant profile of the conductivity suggests the presence of Na^+ and Cl^- ions at high precipitants concentration precluded the expected conductivity decrease.

The differences in the initial and final pH values are also minimal. For instance, when $C_A = 75 \text{ mM}$ and $\tau = 2 \text{ minutes}$, the reaction mixtures pH was measured as ~ 10.5 while that of 10 mM Ca(OH)_2 solution and final suspension were ~ 12.5 and ~ 12.2 , respectively. This is not necessarily an outcome of a reaction, as low pH solutions would naturally reduce the pH of a high pH solution when mixed.

4.4. Adsorption of Additive Ca^{2+} ions on Particles Surfaces

The comparison of the particles ζ -potential at the 8th minute and 3rd hour when $\tau = 9 \text{ seconds}$ (Table 4.1) also indicates that additive Ca^{2+} ions were irreversibly adsorbed on the crystals. A similar observation was made by Chibowski et al. ⁷³, where the particles ζ -potential was reported to be positive and remained constant long after the precipitation reaction had completed. It was attributed to the adsorption of excess Ca^{2+} ions on the usually negatively-charged CaCO_3 particles surfaces.

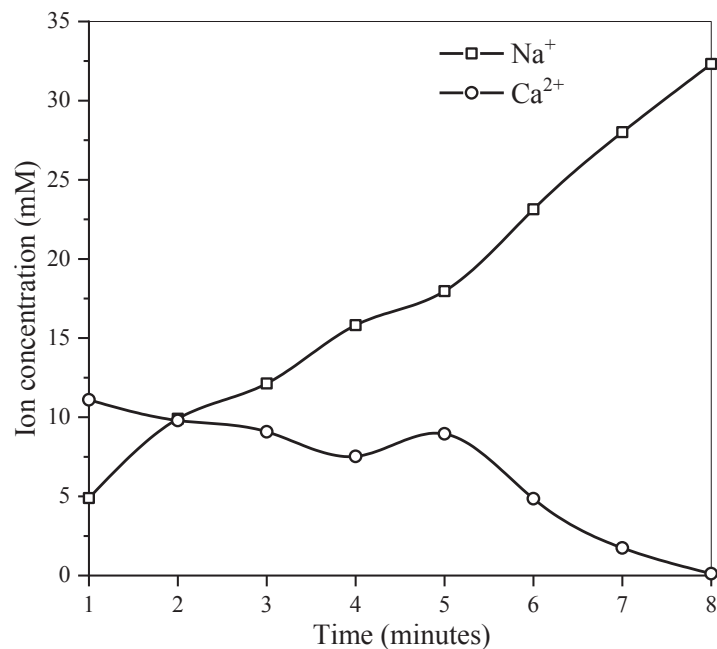


Figure 4.12. Time-dependent changes in the solutions cations concentration when $C_A = 75 \text{ mM}$ and $\tau = 9 \text{ seconds}$.

A total flowrate of $15 \text{ mL}\cdot\text{min}^{-1}$ implies 120 mL of the reaction mixture would have been dispersed in the $\text{Ca}(\text{OH})_2$ solution at the end of the 8th minute. Starting with 250 mL of a 10 mM $\text{Ca}(\text{OH})_2$ solution, the final concentration of the Ca^{2+} ions at the 8th minute would be $\sim 6.8 \text{ mM}$, assuming they were not depleted by electrostatic adsorption on the particles surface. However, the ion chromatography results presented in Figure 4.12 shows the concentration of Ca^{2+} ions generally reduced with time, while Na^+ increased. The concentration of Ca^{2+} in the final suspension was $\sim 0.12 \text{ mM}$, which is approximately equal to the solubility of CaCO_3 , suggesting a complete adsorption of the additive Ca^{2+} ions on the particles.

The difference between the final concentration of additive Ca^{2+} ions obtained by material balance and ion chromatography experiments further proves that, while reactions do not occur in the growth inhibition space, the Ca^{2+} ions preferentially adsorb onto the particles surfaces, thereby increasing electrostatic repulsions for growth inhibition.

4.5. Effects of $\text{Ca}(\text{OH})_2$ Concentration

The fundamental question this section seeks to answer is the extent to which the additive Ca^{2+} ions can inhibit the particles growth. Here, the concentration of the precipitants and starting $\text{Ca}(\text{OH})_2$ solution were varied. Different volumes of the precipitants were reacted in the tubular reactor with $\tau = 9$ seconds, and at the same flowrate. The reaction mixtures were continuously dispersed in a 200 mL stabilizing solution, containing a predefined initial concentration of additive Ca^{2+} ions.

As earlier stated, the dispersion of more precipitates in the growth-inhibiting solution would increase the suspensions volume and result in a decrease in the molar concentration of the additive Ca^{2+} ions, which can be easily determined from material balance, assuming they are not adsorbed from the solution. However, the crystals initial growth rate is higher at high solutes concentration, and a greater amount of larger particles precipitate. This would require the adsorption of more Ca^{2+} ions for sufficient growth inhibition²⁶. Therefore, it is for consistency and ease of reporting that the results are presented in terms of β , as the molar concentration of Ca^{2+} ions in the final suspension would vary, depending on the precipitants concentration and reacted volume, if their

irreversible adsorption on the particles is taken into consideration. Here, β denotes the ratio of the total volume of the reaction mixture to the stabilizing solutions volume.

4.5.1. Particle Growth and Colloidal Stability

Particles sizes and ζ -potentials at different conditions are presented in Table 4.2.

Table 4.2. Particles stability and hydrodynamic sizes.

β	$C_S = 0 \text{ mM}$		$C_S = 5 \text{ mM}$		$C_S = 10 \text{ mM}$		$C_S = 15 \text{ mM}$	
	Size (nm)	Size (nm)	ζ -potential (mV)	Size (nm)	ζ -potential (mV)	Size (nm)	ζ -potential (mV)	
$C_A = 25 \text{ mM}$								
0.5		961.8	20.9	413.2	27.7	290.2	25.5	
1	7107	1421	15.5	467.4	16.1	391.4	21.6	
2		2781	11.9	927.1	18.1	537.3	13.5	
4		9042		3041	-6.7	1116	13.7	
$C_A = 50 \text{ mM}$								
0.5	9192	1169	12.8	622.3	24.3	931	16.5	
1	13470	2436	8.58	1201	20.4	1332	14.7	
2	>18000	9280		3837		7495	12.5	
4	>18000	13450		6831		11840	-8.23	
$C_A = 75 \text{ mM}$								
0.5		1745	15.6	844.1	13.9	2684	27.9	
1	>18000	2768	-10.7	2837		3064	14	
2		12090		5570		10490		
4		15000		11790		13600		

The equilibrium state of a crystal possesses the minimum surface free energy for any given volume. Therefore, surfaces with high free energies would have large growth rates, causing the dispersed particles to agglomerate and sediment in order to minimize their interfacial area to the surrounding dispersion medium^{26, 79}. This was particularly observed in $C_S = 0$ mM cases, as the particles were unstable and settled rapidly, making the ζ -potentials impossible to measure.

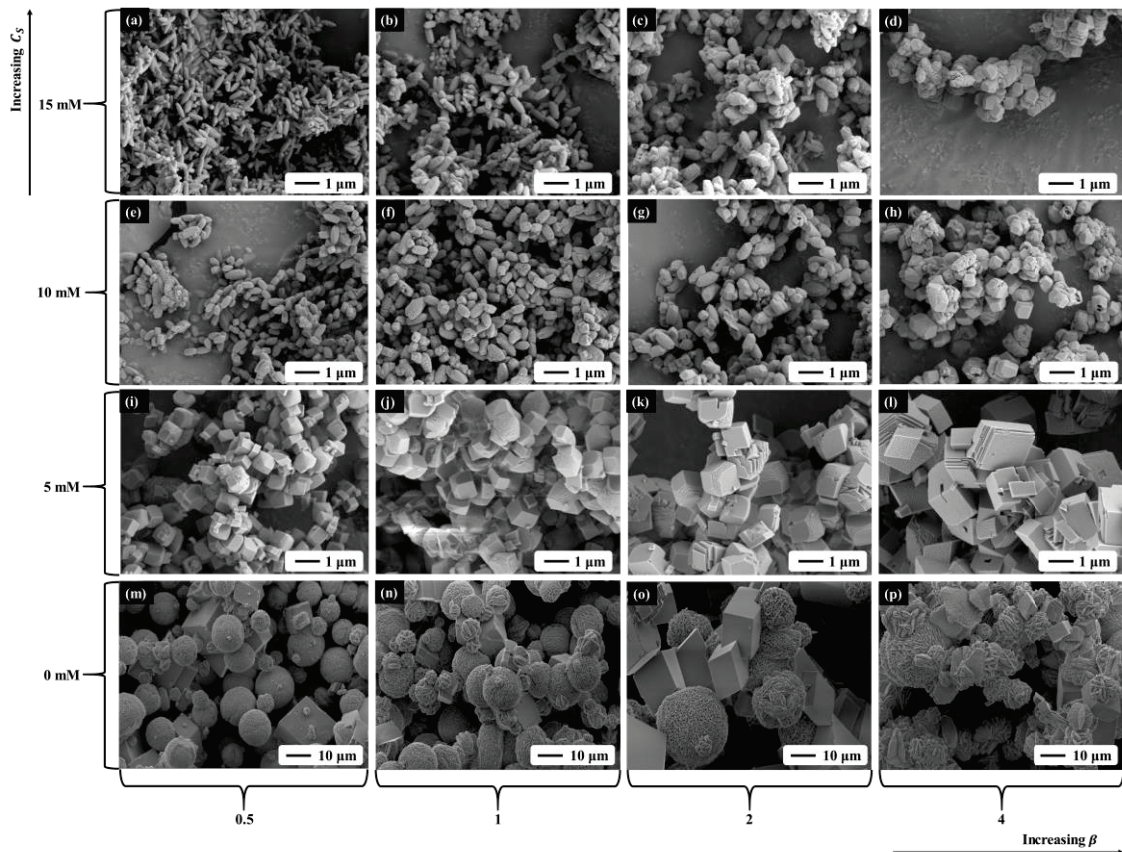


Figure 4.13. Particles morphology as a function of β and C_S for $C_A = 50$ mM.

However, as shown in Table 4.2, the presence of additive Ca^{2+} ions improved the colloidal stability of the particles, as they adsorbed onto the crystals, thereby reducing their surface free energies and tendency to coalesce⁴¹. Figure 4.13, which is a graphical illustration of the SEM photomicrographs for $C_A = 50$ mM, shows that the excessive growth observed when $C_S = 0$ mM was impeded in the presence of additive Ca^{2+} ions, regardless of β .

The hydrodynamic sizes were indeterminable in some $C_S = 0$ mM cases. They were presumed to be larger than the maximum ($18 \mu\text{m}$) measurable by the Coulter

Counter. Although Figure 4.13 shows smaller particles were synthesized as C_S increased; compared to the corresponding values at $C_S = 10$ mM, the particles mean hydrodynamic sizes increased at $C_S = 15$ mM when $C_A = 50$ and 75 mM (Table 4.2). This aberration is considered a result of a known demerit of DLS method, since the SEM micrographs (Figure 4.14b-c) indicate the individual particles sizes reduced. Besides assuming a spherical shape for the dispersed particles, the presence of aggregates in the sample can immensely affects DLS ability to correctly determine the actual size^{24, 77}.

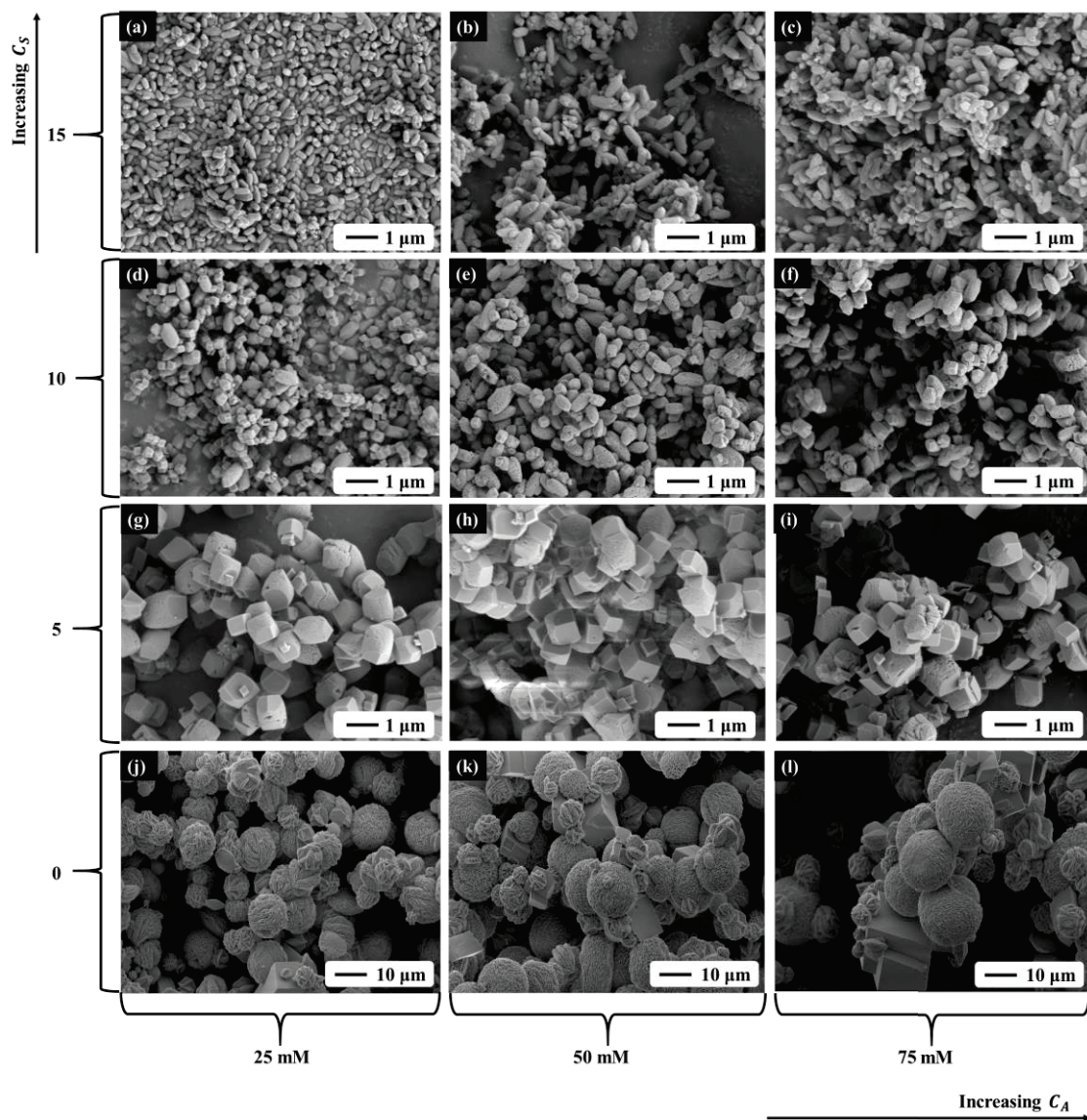


Figure 4.14. Morphology change as a function of C_A and C_S for $\beta = 1$.

SEM micrographs provide reliable information about particle sizes, but the drying process can cause shrinkage which might result in underestimation of the real size

²⁴. Notwithstanding, the formation of large aggregates is evident in Figure 4.13a-d and Figure 4.14b-c. Compared to when $C_S = 10$ mM, this implies the electrostatic repulsions of the charged particles surfaces were weaker at all values of β , for $C_A = 50$ and 75 mM cases when $C_S = 15$ mM. This is evident in the particles loss of colloidal stability, which is demonstrated in ζ -potential decrease under the stated conditions (Table 4.2).

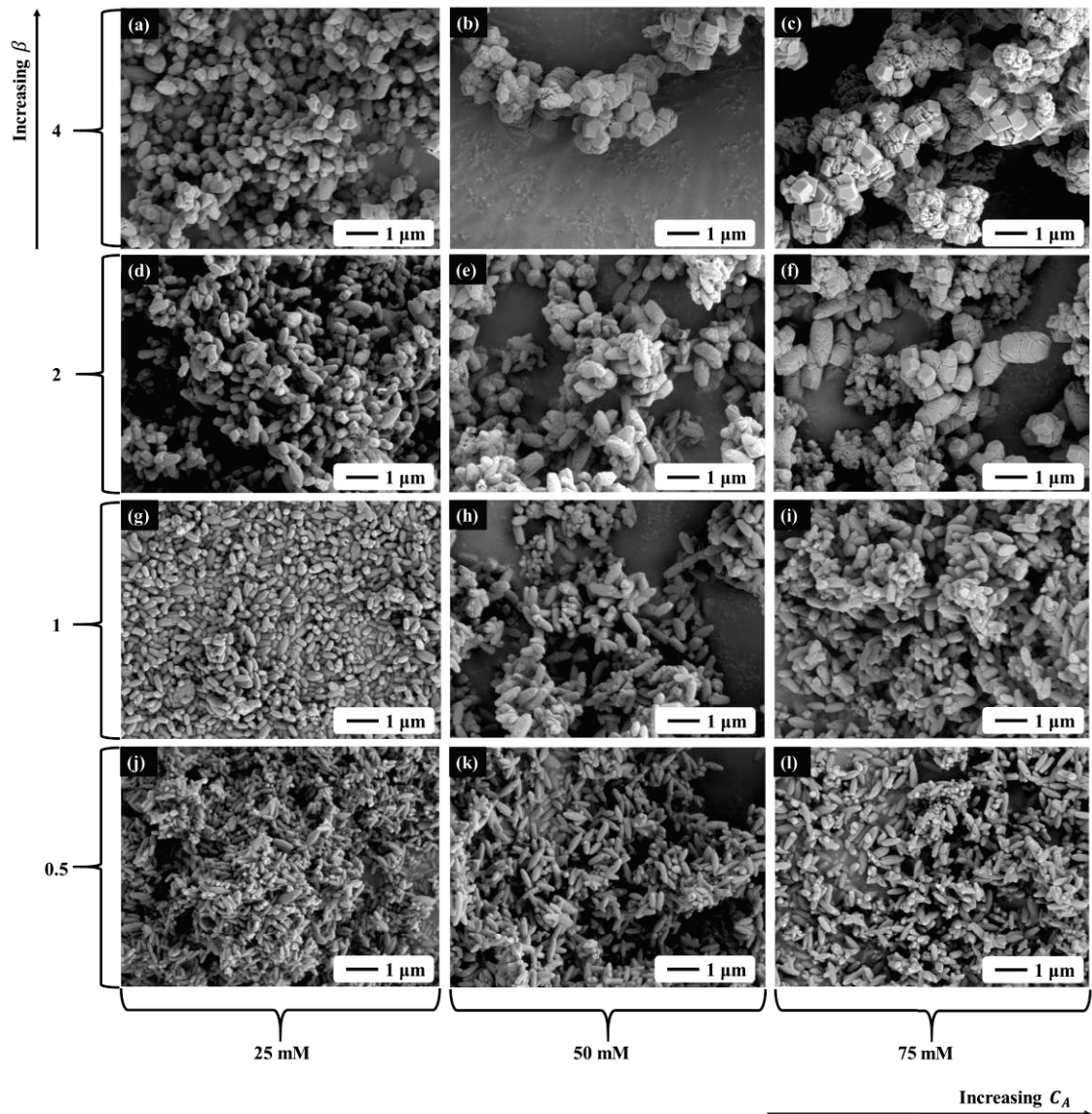


Figure 4.15. Morphology change with respect to β for $C_S = 15$ mM.

Furthermore, it is a likely effect of increased concentration of the precipitants counter ions (Eq. 4.2) in the suspension ⁷⁸. Cheng et al. ²⁹ reported that at higher concentrations, NaCl can cause CaCO_3 particles growth and morphology changes, even in the presence of an inhibitor. However, this was only observed when $C_S = 15$ mM for

$C_A = 50$ and 75 mM cases. Thus, it is interpreted as a possible effect of increased interactions between unlike charges in the solution, at a higher Ca(OH)_2 concentration. For instance, the ζ -potential was highest (27.9 mV) at $\beta = 0.5$, $C_S = 15$ mM and $C_A = 75$ mM. Though agglomerated, Figure 4.15l shows the individual particles were smaller, suggesting the aggregates formed stable clusters in the suspension.

The greatest growth inhibitory effects of additive Ca^{2+} ions were observed at $C_S = 15$ mM for all values of β at $C_A = 25$ mM (Table 4.2). With $\beta = 1$, the particles mean hydrodynamic size reduced from ~ 7 μm to ~ 1.4 μm when $C_S = 5$ mM. It further decreased to ~ 400 nm when C_S was increased to 15 mM. This is $\sim 95\%$ reduction in the sizes of the particles that was produced in the absence of additive Ca^{2+} ions. It is in agreement with previous studies which show that higher concentrations of additives is necessary for substantial retardation of CaCO_3 crystals growth^{26, 29, 81}. Increasing the concentration of Ca^{2+} ions in the stabilizing solution improved the particles ζ -potential, especially at low β .

4.5.2. Polymorphic Transformation

The XRD pattern of the particles synthesized at different C_S for $C_A = 50$ mM and $\beta = 1$, presented in Figure 4.16, shows that vaterite CaCO_3 polymorph was only formed at $C_S = 0$ mM. Irrespective of β and C_A , Rietveld refinement revealed the vaterite phase was more than 70% of the particles produced in $C_S = 0$ mM cases. Figure 4.13(m-p) confirms the presence of calcite polymorph as well-developed faceted rhombohedra while the spherical particles are observed to be composed of smaller growth units, which is a phenomenon peculiar to polycrystalline vaterite^{6, 14, 34, 82}.

As amorphous CaCO_3 (ACC) is known to transform into calcite through a vaterite intermediate at ambient temperature, the formation of calcite is affected by factors such as ageing time, temperature and presence of foreign ions or organic molecules. In the current study, pure calcite phases were formed when additive Ca^{2+} ions were present in the stabilizing solution. This is consistent with previous studies which show excess Ca^{2+} ion to favor direct precipitation of calcite without a metastable intermediate^{1, 3, 55}.

Furthermore, the amount of vaterite in the particles synthesized at $C_S = 0$ mM and $\tau = 2$ minutes (Figure 4.8) is less, compared to those obtained in $\tau = 9$ seconds cases (Figure 4.16). Rietveld refinement revealed the particles contained $\sim 34\%$ and more than

70% vaterite, when $\tau = 2$ minutes and 9 seconds respectively. Since the polymorphic transformation is solution mediated, this implies that the particles had more time, in the $\tau = 2$ minutes case, to transform into calcite in the tubular reactor^{6, 9, 39, 76}. This is a natural phenomenon which proceeds faster under conditions of high supersaturation, making the occurrence or synthesis of pure vaterite phases elusive^{14, 34, 83-84}.

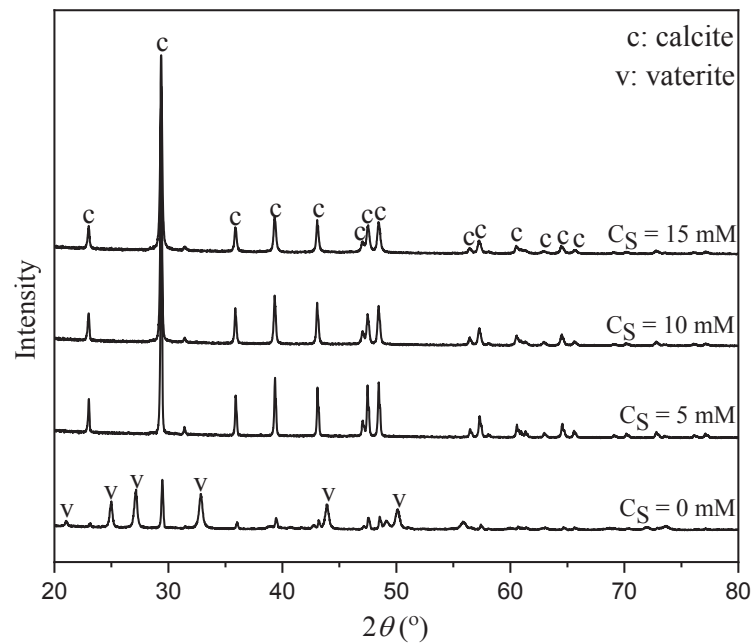


Figure 4.16. Crystal form with respect to C_S for $C_A = 50$ mM.

4.5.3. Alteration of Particles Morphology

The particles morphology also changed with increasing C_S , depending on β . For instance, when $C_A = 50$ mM and $\beta = 0.5$, the sample was predominantly vaterite spheres at $C_S = 0$ mM (Figure 4.13m), but changed to truncated cubes at $C_S = 5$ mM (Figure 4.13i), a mix of different structures at $C_S = 10$ mM (Figure 4.13e), and fairly monodispersed scalenohedral particles at $C_S = 15$ mM (Figure 4.13a). Cizer et al.³ also showed that ACC morphs into scalenohedral calcite in excess Ca^{2+} ions conditions.

In addition, an aggregated mix of rhombohedral calcite and spherical vaterite particles were synthesized at $C_S = 0$ mM and $\beta = 4$ (Figure 4.13p) while agglomerated cubic and plate-like calcite particles were formed at $C_S = 5$ mM (Figure 4.13l). Chain-like aggregates of truncated cubes were obtained when C_S was increased to 15 mM (Figure 4.13d).

Since Ca^{2+} ions selectively adsorb on the crystals surfaces to poison the growth sites, the agglomerated and less monodisperse cases with a combination of different morphologies observed in Figure 4.13 is explained as a consequence of different growth rates of the crystals faces. It indicates instances of insufficient additive Ca^{2+} ions which resulted in reduced electrostatic repulsions and also weakened the growth inhibition process^{28-29,41}. It is an outcome of the depletion of the additive Ca^{2+} ions, as they adsorb on the earliest precipitates.

4.5.4. Changes in Particles Specific Surface Area

The presence of additive Ca^{2+} ions also affected the particles specific surface area (SSA). Surface area analyses showed the particles have an average pore width of ~ 5 nm. The BET particle SSA $\beta = 1$ cases at different C_A , are presented in Figure 4.17. The large size, spongy and framboidal nature of the spherical vaterite particles, as observed in Figure 4.14, could account for the large BET SSA recorded in the absence of additive Ca^{2+} ions when $C_A < 75$ mM^{14,38}. Agnihotri et al.⁸⁵ reported that the rapid aggregation of crystals nuclei, due to low electrostatic repulsions in the absence of charged foreign substances, provides an open pore structure with high surface area and volume in precipitated CaCO_3 particles.

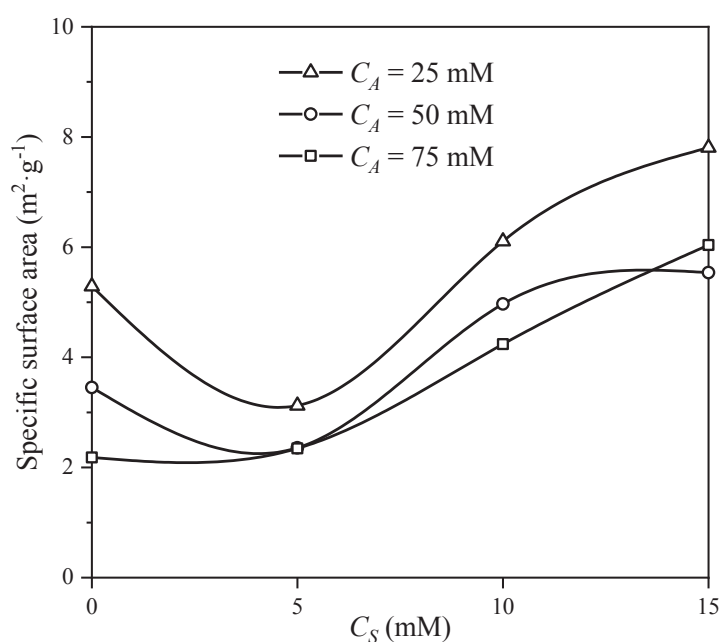


Figure 4.17. Effects of C_S on particles BET SSA when $\beta = 1$.

The crystals seem to have been more compact at higher precipitants concentration, especially when $C_S = 0$ mM. Despite their large sizes, precipitated vaterite particles are often made up of crystallites with sizes between 25 – 35 nm⁸⁶. Therefore, increased concentration of solutes ions would have resulted in the precipitation of more crystallites which could have been more closely packed, providing a smaller open pore structure. This explains why, as shown in Figure 4.17, the SSA at $C_S = 0$ mM was highest when $C_A = 25$ mM and lowest when $C_A = 75$ mM, even though the particles were larger. Thus, CaCO₃ particles SSA decreases with increasing size¹⁴.

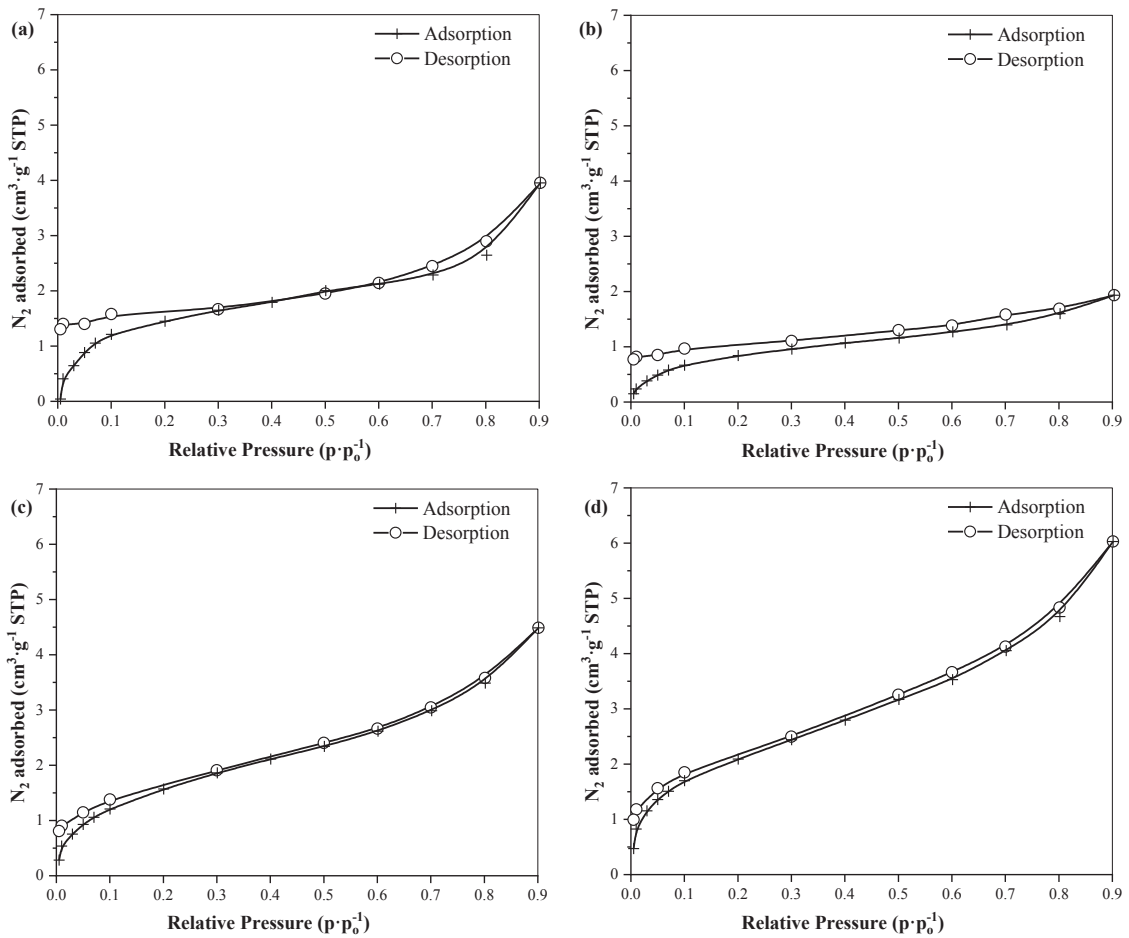


Figure 4.18. Isotherm linear plot of particles synthesized when $C_A = 25$ mM, $\beta = 1$ and $C_S =$: (a) 0 mM; (b) 5 mM; (c) 10 mM; (d) 15 mM.

From Figure 4.17, when $C_S = 5$ mM and $C_A < 75$ mM, the particles SSA slightly reduced just as their growth was inhibited. Further increasing C_S intensified the corrosion of the particles surface and increased the SSA. The same SSA changes with respect to C_S when $C_A = 25$ mM was also observed when $C_A = 50$ mM. However, unlike the case at

lower C_A , initial reduction in the particles SSA, at $C_S = 5$ mM, is not observed when $C_A = 75$ mM. Notwithstanding, the SSA increased as C_S increased, despite a significant decrease in the particles size.

The presence of pores in these particles is also demonstrated by the hysteresis in the $N_{2(g)}$ adsorption-desorption isotherm (Figure 4.18). For low C_S cases, while the hysteresis was widest at low relative pressures, the particles adsorbed less amounts of $N_{2(g)}$ at high pressures. The highest extent of adsorption was observed in particles synthesized when $C_S = 15$ mM because of the higher SSA which is due to a larger pore structure. The increased intensity of pores in the particles at high additive Ca^{2+} ions concentration is also evident in the SEM micrographs (Figure 4.14).

Compared to the case when $C_S = 0$ mM, the particles adsorbed even lesser amounts of $N_{2(g)}$ when $C_S = 5$ mM. This is both due to the reduction in the particles size and SSA as observed in Table 4.2 and Figure 4.17, respectively. Moreover, larger particles with more open pore structure would adsorb more.

The crystallization of pure calcite phases in the presence of additive Ca^{2+} ions implies the growth-inhibiting solution will be saturated with calcite. The pH of the reaction mixtures were ~ 10.5 while that of a 5 mM $Ca(OH)_2$ solution was ~ 12.1 , and differences in the initial and final pH values after the process were nominal. These make no case for particle dissolution as the binding energy of lattice Ca^{2+} and CO_3^{2-} ions is also high in elevated alkaline conditions³⁶. Moreover, calcite is the most stable $CaCO_3$ polymorph and has the lowest solubility product ($K_{sp} = 10^{-8.48}$). Since additive Ca^{2+} ions are foreign to the crystal lattice, it is more likely that the occurrence of pores in the particles is a result of dislocations caused by abrupt morphology changes, polymorphic transformation or complete growth inhibition at specific sites in the crystals.

4.6. Precipitants Concentration and Volume Effects

The particles were expected to grow larger with increasing C_A , since the initial growth rate of crystals increases at higher degrees of supersaturation^{26, 28, 39, 41}. This also suggests the sizes will increase as more reaction mixture containing a higher concentration of solutes is fed into the growth-inhibiting solution. As presented in Table 4.2, when $C_S = 0$ mM and $\beta = 1$, the particles hydrodynamic sizes increased from ~ 7 μm

at $C_A = 25$ mM, to $>18 \mu\text{m}$ when C_A was increased to 75 mM. For $C_A = 50$ mM case, the size went from $\sim 9 \mu\text{m}$ when $\beta = 0.5$, to $>18 \mu\text{m}$ at $\beta = 4$.

Despite increasing C_S , Figure 4.14 shows the particles grew as C_A increased when $\beta = 1$. The same is observed in Figure 4.15 which clearly illustrates that the inhibitory efficiency of the additive Ca^{2+} ions decreased at higher C_A and β . It is because they were adsorbed on the earliest particles, thereby reducing the amount available for subsequent precipitates. Thus, the growth-inhibitory effect of the $\text{Ca}(\text{OH})_2$ solution would be lost at high β . Particularly at $C_A > 25$ mM, Figure 4.15 suggests the possibility of obtaining monodisperse nanoparticles reduces when $\beta > 1$. Nonetheless, the particles mean sizes were still less than those obtained in $C_S = 0$ mM cases.

Figure 4.13, Figure 4.14 and Figure 4.15 also show that particle agglomeration intensified as β and C_A increased. This explains why large hydrodynamic sizes were measured in some cases (Table 4.2) while the SEM micrographs displayed a $1 \mu\text{m}$ scale bar. For instance, relatively small rhombohedral particles formed large chain-like aggregates at $C_S = 15$ mM, $C_A = 75$ mM and $\beta = 4$ (Figure 4.15c). However, they were spindle-like scalenohedral crystals when $\beta = 0.5$ (Figure 4.15l). This further intimates that, for any volume of precipitated particles, effective growth inhibition and monodispersity are functions of the amount of Ca^{2+} ions available to adsorb onto the particles.

The colloidal stability of the particles generally declined at higher values of β (Table 4.2). It confirms increase in particles hydrodynamic sizes as a consequence of excessive aggregation. Since more crystals nucleate at higher solutes concentration and volume, the higher number of large crystals and growth sites would necessitate the adsorption of more Ca^{2+} ions. This drastically reduced the concentration of additive Ca^{2+} ions available for growth inhibition as more precipitates reached the stabilizing solution. Consequently, to lower the interfacial tension and achieve equilibrium, the particles started sedimenting the moment the desired volume of precipitants were reacted and stirring was stopped.

High concentration of lattice ions in crystallization processes has been shown to preclude the adsorption of additive ions on crystals surfaces. The high number of solutes collision in such situations can prevent the ions from adsorbing onto the crystals and/or poisoning the growth sites⁴¹. However, the experimental setup designed for this study avoids such a scenario as the nucleation step was separated from the growth inhibition

region where Ca^{2+} ions were waiting as impurities (Figure 3.1). Therefore, the irreversible adsorption of additive Ca^{2+} ions on previously-formed particles growth sites, and increased concentration of counter ions in the system, is believed to have engendered the particles loss of colloidal stability and the resultant agglomeration observed at high β and C_A .

4.7. Synthesizing Stable Monodisperse Calcite Nanoparticles

The procedure described in this study is not without precedents. Kontrec et al.²⁷ showed how the sizes of CaCO_3 particles can be reduced using different polysaccharides. An optimum 50% growth inhibition (16 μm to 8 μm) was obtained with a high molecular weight dextran. Unlike the approach presented here, the use of such organic compounds, polymer or solvents as growth inhibitors may necessitate advanced purification techniques.

The growth of CaCO_3 crystals is spontaneous and rapidly attains equilibrium. A common approach to synthesize small particles is to lower the degree of supersaturation. For instance, Wei et al.¹⁹ prepared ~500 nm vaterite spheres by mixing 2 mM solutions of Na_2CO_3 and CaCl_2 at 30 °C. But the high point of the procedure described in this study is a simple method to produce CaCO_3 nanoparticles under relatively high supersaturation conditions. As observed from the SEM micrographs, it offers a way of synthesizing monodisperse nano- CaCO_3 particles in a reaction involving Na_2CO_3 and CaCl_2 solutions of equimolar concentrations, up to 75 mM.

The extent of growth inhibition depends on the volume of precipitate and concentration of additive Ca^{2+} ions in the stabilizing solution. As presented in Figure 4.19, just as the monodispersity, the particles morphology and size also changed concurrently as C_S increased. From Table 4.2, when $C_A = 25$ mM and $\beta = 0.5$, ~400 and ~300 nm particles were obtained with $C_S = 10$ and 15 mM, respectively. These slightly increased to ~470 and ~400 nm when β was increased to 1. In fact, it is still more than 90% reduction of what the particles sizes would have been in the absence of additive Ca^{2+} ions (~7 μm).

The particles size distribution (Figure 4.20) is monomodal. It does not suggest the presence of aggregates in the suspensions. The width of the distributions is also small, showing that monodispersed CaCO_3 nanoparticles can be synthesized when the volume

of precipitated particles is low or the additive Ca^{2+} ions concentration is high. However, the limited solubility of $\text{Ca}(\text{OH})_2$ in H_2O at ambient temperature is a major drawback in the deployment of the method described herein.

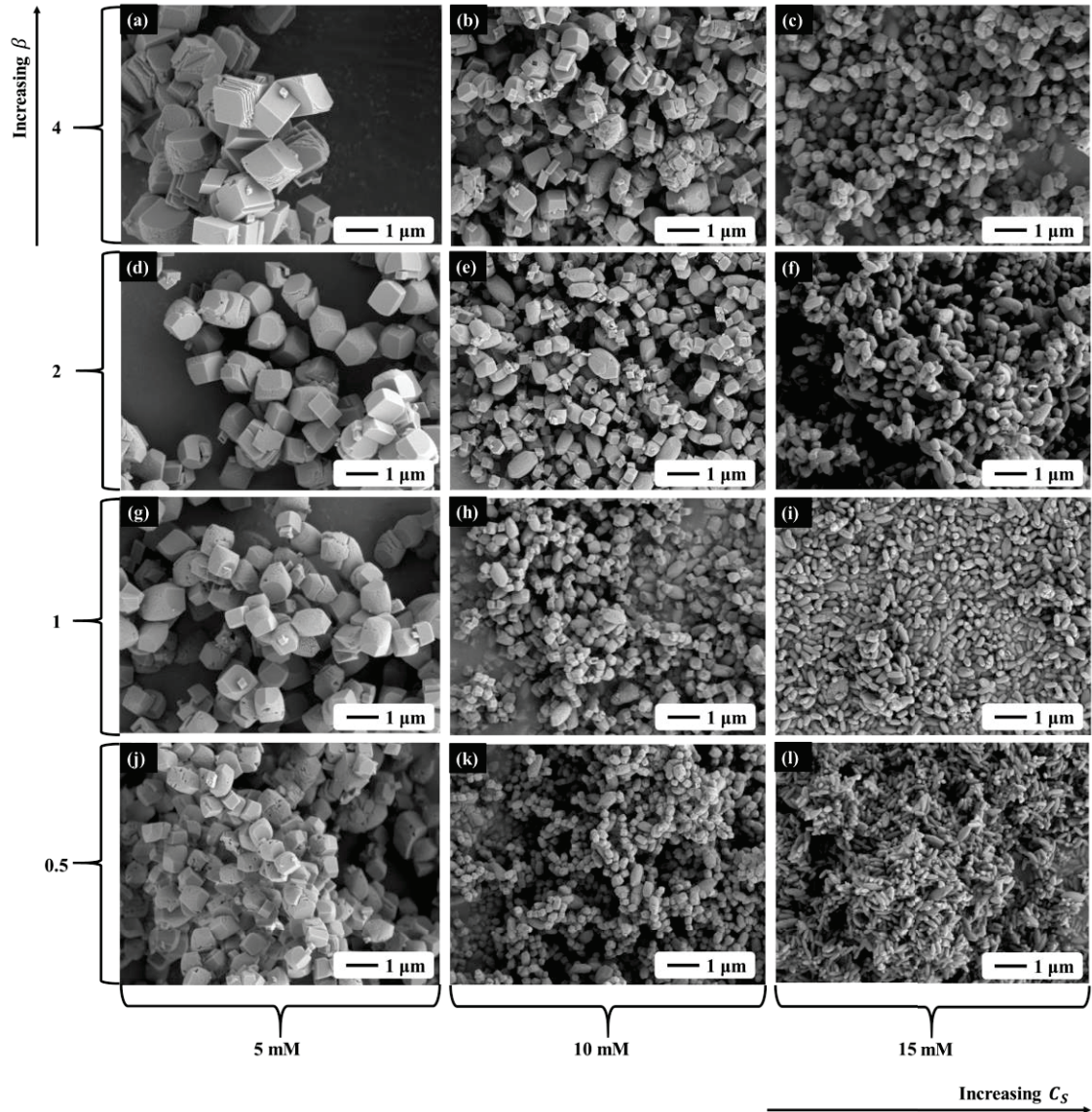


Figure 4.19. Growth inhibition and morphology change for $C_A = 25$ mM.

Even when the volume of precipitates is low, particles synthesized at high precipitants concentration would be large, since the degree of supersaturation is a primary factor affecting the crystals initial growth rate^{19,26}.

Jung et al.⁸⁷ reported that Na^+ ion has significant effects on the morphology and growth of CaCO_3 crystals. This is an important consideration, as Na^+ ion is a byproduct of the studied reaction (Eq. 4.2). However, besides the size and morphology, the presence

of additive Ca^{2+} ions also influenced changes in other particle properties examined. Therefore, the observations in this study cannot be attributed to the presence of Na^+ ions.

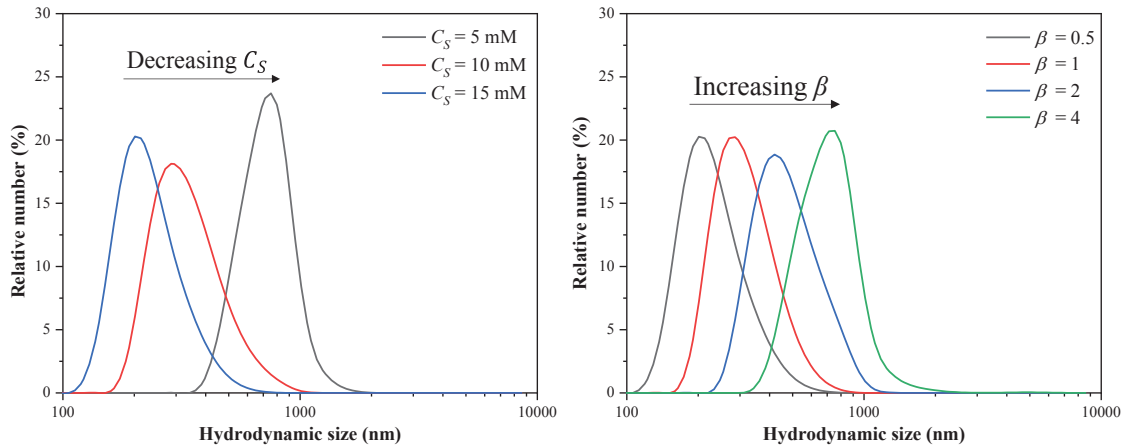


Figure 4.20. Particles size distribution for $C_A = 25$ mM: (a) Effects of C_S when $\beta = 0.5$; (b) Effects of β when $C_S = 15$ mM.

4.8. Stabilizing Solutions Initial pH Effects

It is imperative to understand the effects of pH changes in the growth inhibition region. Here, the starting pH of 200 mL of 10 mM $\text{Ca}(\text{OH})_2$ solution was adjusted with HCl acid to a predefined value. 50 mL of each precipitant with $C_A = 25$ mM was reacted in the tubular reactor with $\tau = 9$ seconds, and dispersed in the stabilizing solution. The particles properties were compared with those synthesized when pure H_2O , and NaOH solution with initial pH ≈ 13 were used in place of $\text{Ca}(\text{OH})_2$.

4.8.1. Crystal Form

The concentration of OH^- ions also contributes to the polymorphic transformation of freshly-precipitated CaCO_3 particles. Previous studies show that calcite predominates at high pH, regardless of the concentration of impurity ions^{1, 88}. Likewise, as illustrated in Figure 4.21, a pure calcite phase was produced when NaOH solution with initial pH ≈ 13 was used, while a mixture of vaterite and calcite was obtained in pure H_2O , where the suspensions pH rapidly increased to a final value of ~ 10.5 .

Rietveld refinement showed that particles synthesized in NaOH and H_2O were $\sim 100\%$ and $\sim 70\%$ calcite, respectively. In moderately basic solutions containing no

impurity ions, the growth of calcite follows a surface-controlled dissolution-recrystallization pathway via vaterite, at ambient temperature^{1, 89-90}. This suggests the vaterite crystals obtained in the pure H₂O case will eventually transform into calcite, if left in suspension for a much longer time⁹¹.

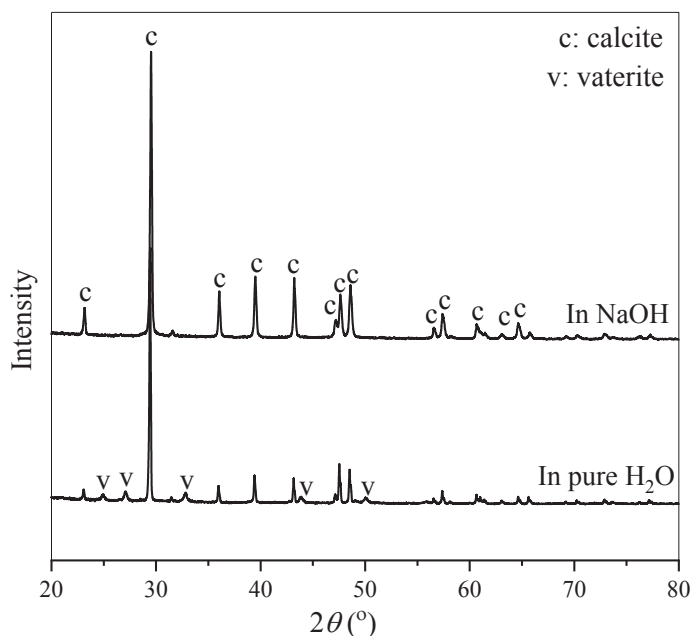


Figure 4.21. Crystal form of particles obtained when growth inhibition was attempted in both NaOH solution with initial pH \approx 13 and pure H₂O.

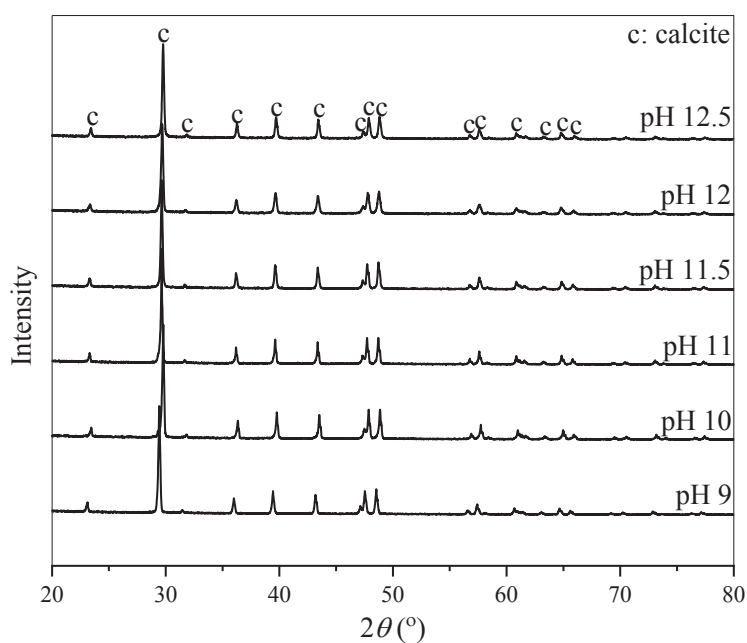


Figure 4.22. Stabilizing solutions initial pH effects on crystals form when $C_A = 25$ mM, $C_S = 10$ mM and $\beta = 0.5$.

In contrast, the X-ray diffractograms presented in Figure 4.22 demonstrate that pH variations had no effect on the crystal form of the synthesized particles, when additive Ca^{2+} ions were present in the suspension. Rietveld refinement of the XRD data showed pure calcite phases crystallized, irrespective of the suspensions pH – even at relatively low pH levels known to favor the crystallization of vaterite^{1, 90}. This confirms that, besides a high pH condition, additive Ca^{2+} ions also influence the particles crystal structure. A similar observation was reported in Rodriguez-Blanco et al.⁹⁰ where Mg^{2+} ion, regardless of differences in the solutions pH, caused the crystallization of calcite at conditions favorable to the precipitation of metastable vaterite.

4.8.2. Particles Size and Morphology

Figure 4.23 shows that nanoparticles were synthesized when the initial pH was 12.5 and 12. The particles, however, overgrew as the pH was further reduced, approaching $4.5 \mu\text{m}$ at pH = 9. This is also observed in the SEM micrographs (Figure 4.24) and indicates that the additive Ca^{2+} ions lost their growth inhibitory efficiency in low pH conditions. It is interpreted as a consequence of the particles ionic speciation as they arrived in the stabilizing solution, since the binding tendency of Ca^{2+} and CO_3^{2-} ions is known to decline in low pH media^{36, 73}. The dissolution of the particles seemed to wane as more precipitates reached the solution, leaving fragmented pieces which subsequently aggregated (Figure 4.24).

The solutions initial pH also affected the morphology and monodispersity of the particles. Fairly monodispersed truncated cubes were synthesized at pH = 12.5 (Figure 4.24a), but erosion of the particles surfaces and pits formation, which signifies a case of weak dissolution, is observed when the pH was reduced to 12. Figure 4.24(b-c) reveals the truncated cubes were dissolving from the curved edges to form well-faceted rhombohedra which suffered edge dislocation defects as the pH was further lowered. The fragments and rectangular slabs seen in the samples are presumed to be remnants of the dissolution process.

Contrary to the observations when additive Ca^{2+} ions were present in the suspension, Figure 4.25 indicates the particles grew uninhibitedly when NaOH solution and pure H_2O were used as the stabilizing solution. In both cases, the samples were highly polydisperse and the hydrodynamic mean sizes were $\sim 5 \mu\text{m}$, despite the wide difference

in pH. This leads to the conclusion that Na^+ ions have no influence on the particles growth, and a high pH condition and the presence of additive Ca^{2+} ions is a necessity for growth inhibition and particles monodispersity.

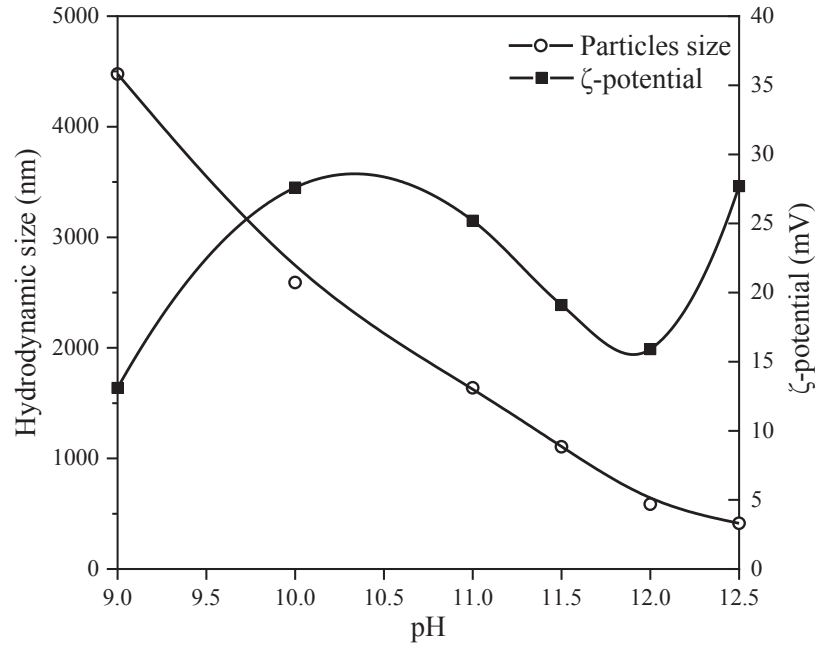


Figure 4.23. Particles hydrodynamic sizes and ζ -potential changes at different pH when $C_A = 25$ mM, $C_S = 10$ mM and $\beta = 0.5$.

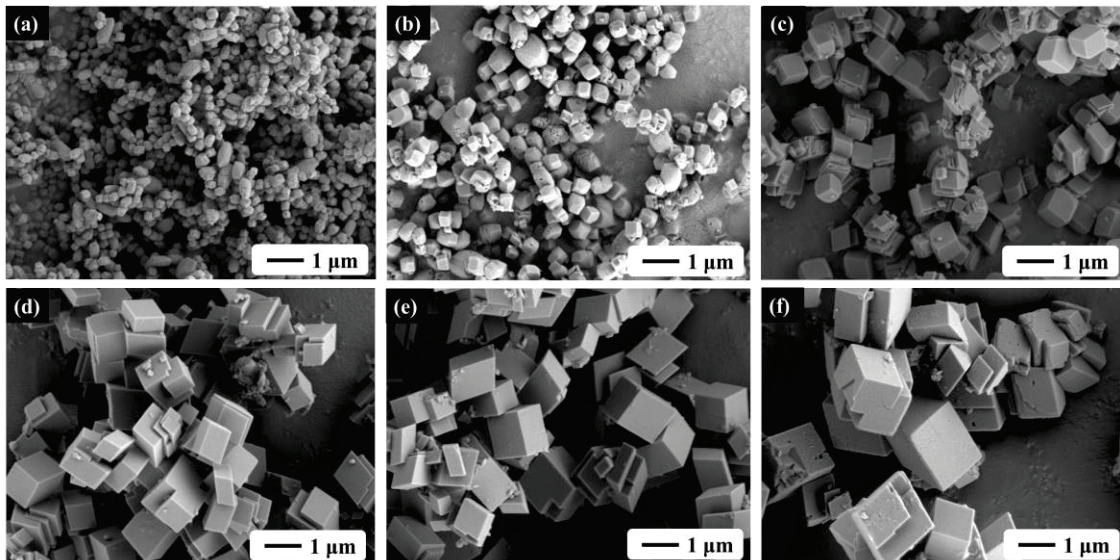


Figure 4.24. Stabilizing solutions initial pH effects on particles morphology when $C_A = 25$ mM, $C_S = 10$ mM and $\beta = 0.5$. pH = (a) 12.5; (b) 12.0 (c) 11.5; (d) 11.0; (e) 10.0; (f) 9.0.

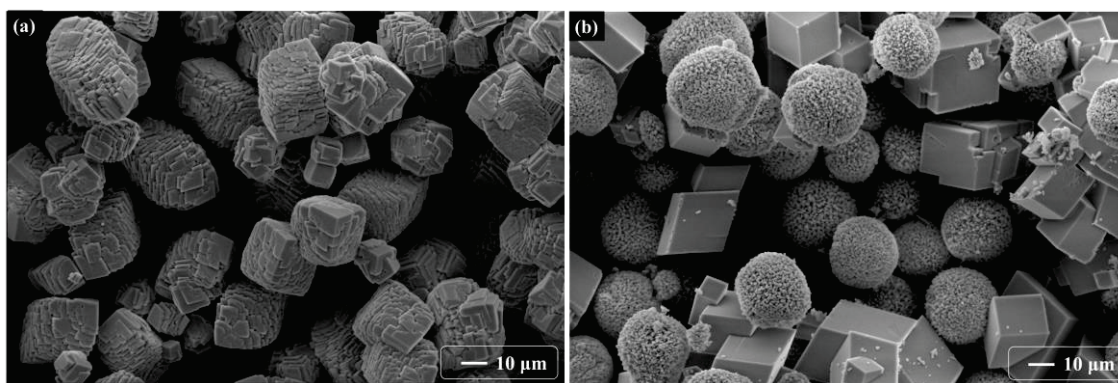


Figure 4.25. Morphology of particles synthesized when growth inhibition was attempted in: (a) NaOH solution with initial pH \approx 13; and (b) pure H₂O.

From Figure 4.25, the particles however have distinct morphologies. While they are a commingling of fully-developed rhombohedra calcite and spherical vaterite in the H₂O case, they appear as laminated cubic structures in the NaOH solution case.

4.8.3. Particles Colloidal Stability and Specific Surface Area

The ζ -potentials of the particles synthesized at pH = 10 and 11 (25.2 and 27.6 mV respectively) indicate they were relatively stable, despite the overgrowth and agglomeration observed in the SEM micrographs (Figure 4.24d – e). It suggests the aggregates exhibited more strongly-charged surfaces compared to what was obtained with initial pH = 12. This can be attributed to the reduction in the amount of particles in the stabilizing solution due to dissolution and the relative increase in the concentration of free Ca²⁺ ions in the suspension, which enhanced the electrostatic repulsions of the already aggregated particles surfaces.

Table 4.3. Particles ζ -potential and hydrodynamic sizes in different stabilizing solutions.

Solution	Initial pH	Final pH	Particles size (nm)	ζ -potential (mV)
Ca(OH) ₂	12.5	12.3	413.2	27.7
NaOH	12.9	12.7	5629	-7.6
H ₂ O	5.9	10.6	5347	

With increased solubility in low pH conditions, the dissolution of CaCO_3 particles gives off $\text{CO}_2(\text{g})$, leaving comparatively more Ca^{2+} ions in the solution. After the equilibration of $\text{H}_2\text{O}/\text{CaCO}_3$ systems, possible reactions that occur, according to Somasundaran and Agar ⁹² is presented in Eqs. 4.3 – 4.7.

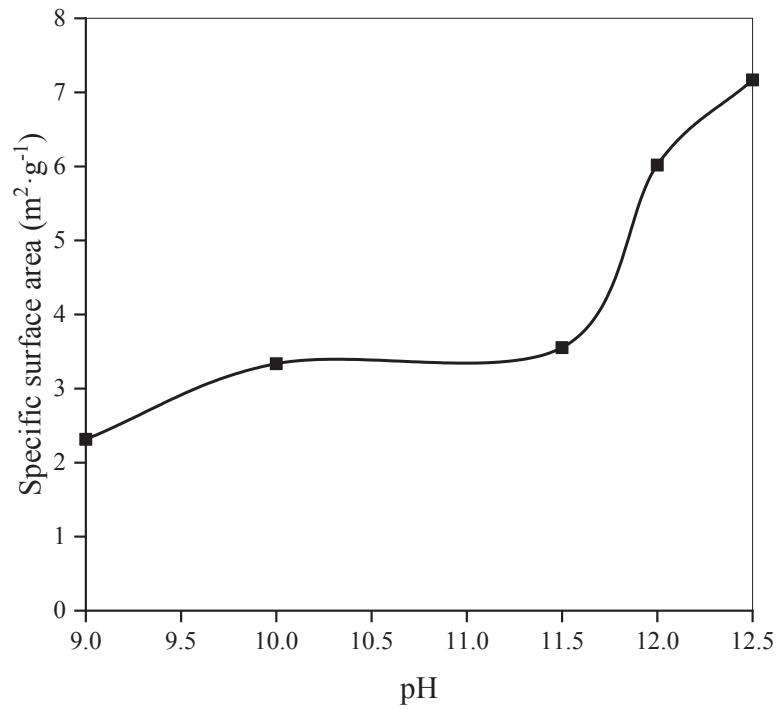


Figure 4.26. Particles BET SSA at different initial pH.

The particles synthesized when initial pH = 9 were relatively unstable in the suspension. This is supported by the increased magnitude of agglomeration and particles size observable in Figure 4.24f. The isoelectric point (IEP) of calcite is reported to between a pH of 8.2 and 8.4 ⁹². This range is approximately close to the final suspensions pH, which was measured as ~8.6. Since IEP is the pH at which ζ -potential is zero, the particles could not have attained colloidal stability in this specific condition without the

influence of foreign ions. The steep drop in the ζ -potential to ~ 13 mV, when initial pH = 9, also explains the increase in the particles size.

In a condition of excess Ca^{2+} ions, pH changes in the stabilizing solution is not expected to alter the electric charge of the particles ζ -potential, nor completely reduce it to zero. As the surface of calcite is known to be negatively charged, the positive value of the synthesized particles ζ -potentials informs that the additive Ca^{2+} ions adsorbed on the particles surfaces, regardless of the solutions pH^{31, 72-73, 78, 93}.

However, the particles synthesized in NaOH solution and H₂O were highly unstable and settled rapidly. From Table 4.3, the ζ -potential of the particles in the NaOH case was -8 mV. Unlike Ca^{2+} ions, it indicates Na^+ ions cannot adequately adsorb on the particles. Therefore, Na^+ ions cannot provide the electrostatic repulsions needed to obtain nano- CaCO_3 particles.

Although the particles obtained in lower initial pH conditions were larger, and would have higher surface areas, Figure 4.26 shows the BET SSA decreased as the solutions initial pH decreased. It indicates the crystallites were more densely packed in low pH conditions. This is also evidenced in the SEM micrographs (Figure 4.24), which show the rhombohedra particles produced when initial pH ≤ 11.5 were nonporous and possessed smooth faces.

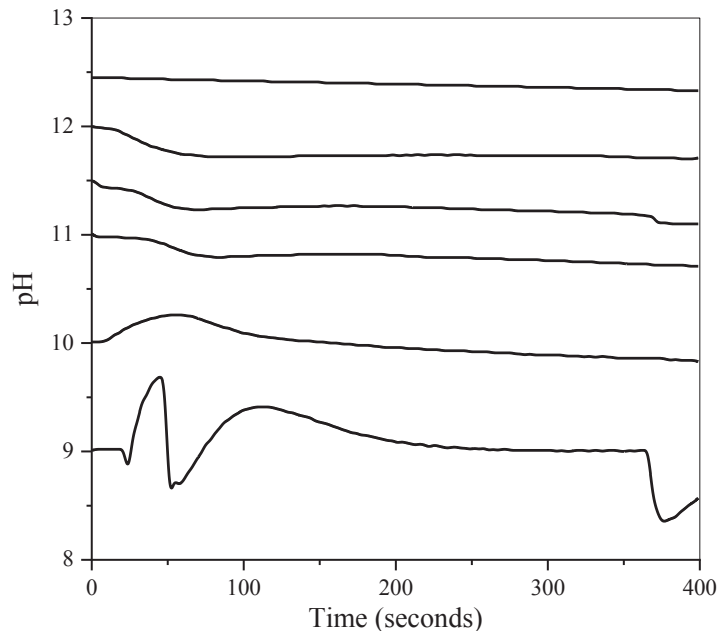


Figure 4.27. Stabilizing solutions pH changes for different initial pH when $C_A = 25$ mM, $C_S = 10$ mM and $\beta = 0.5$.

4.8.4. Changes in Suspensions pH

Figure 4.27 shows the solutions pH slightly reduced in all the studied cases. Without pH adjustment ($\text{pH} \approx 12.5$), the suspensions pH decreased in an almost linear form. This pH decrease follows a natural course. It is due to the dispersion of a lower pH solution (reaction mixture) in a higher one (growth-inhibiting solution). The pH of the reaction mixture was measured as ~ 10.5 , and for $11 \leq \text{pH} \leq 12$ cases, the suspensions pH steadily decreased within the first 100 seconds and remained fairly constant the rest of the time.

When initial $\text{pH} = 10$, the suspensions pH initially increased as a result of the slightly higher pH of the reaction mixture. However, increasing concentration of HCO_3^- ion due to CaCO_3 particles dissolution is believed to have caused the subsequent decrease. Moreover, HCO_3^- ion is the predominant CO_3^{2-} ion species in low pH conditions^{53, 88}.

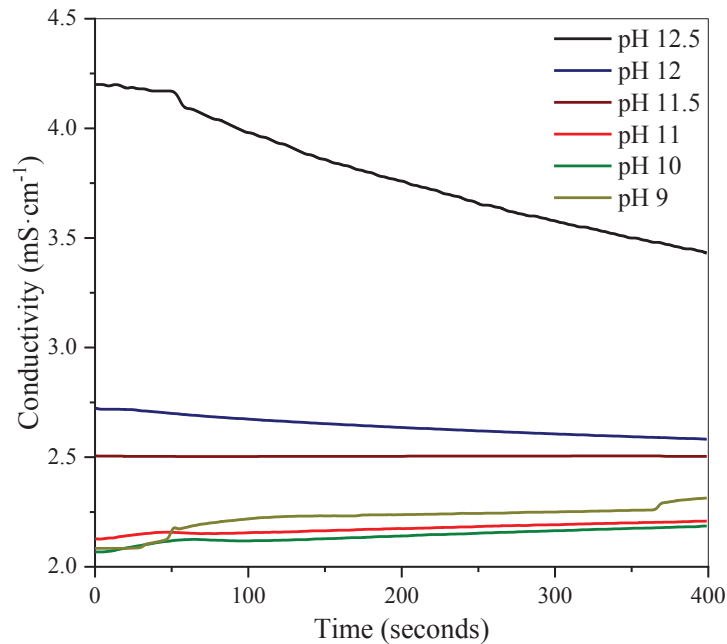


Figure 4.28. Solutions conductivity changes for different initial pH when $C_A = 25$ mM, $C_S = 10$ mM and $\beta = 0.5$.

Similarly, fluctuations in the pH observed in the first 2 minutes, when initial $\text{pH} = 9$, is representative of a suspension system spontaneously equilibrating as more particles precipitated and some concurrently dissolved. Continuous flow of the

precipitates into the solution seemed to have kept the suspensions pH from decreasing at the rate it would have. Despite having a pH lower than the reaction mixtures, the suspensions pH remained constant for a greater part of the duration. With respect to the dissolution mechanism presented in Eqs. 4.3 – 4.7, the later dip is also interpreted as an effect of increased HCO_3^- ion concentration in the system as more particles would have dissolved.

As presented in Table 4.3, the pH change was insignificant when NaOH solution was used: it steadily decreased from 12.9 to 12.7. But in the pure H_2O case, it increased from ~6 to ~10.5 immediately the first precipitates were dispersed. CaCO_3 , being a basic salt, produces a solution with equilibrium pH ≈ 10.3 , when dissolved in H_2O at room temperature. CaCO_3 is only sparingly soluble, and the mixture of the precipitates solution containing scarcely dissolved CaCO_3 , with the stabilizing solution is considered the reason for the pH increase in the H_2O case.

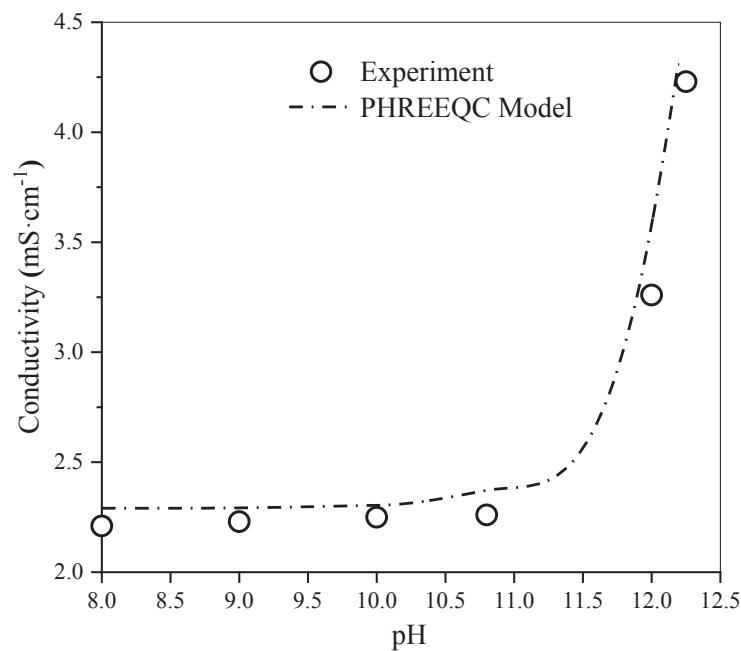


Figure 4.29. Relationship between the pH and conductivity of 10 mM $\text{Ca}(\text{OH})_2$ solution.

4.8.5. Changes in Suspensions Conductivity

Changes in the solutions conductivity for the duration of the process and at different initial pH is presented in Figure 4.28. If complete reaction (Eq. 4.2) is assumed, depending on the pH, conductivity changes can either be a result of the increasing

concentration of Na^+ and Cl^- ions, dissolution of precipitated CaCO_3 particles, and/or decreasing molar concentration of Ca^{2+} ions in the suspension as volume increases with more precipitates being fed in.

Figure 4.28 shows the initial values of the solutions conductivity at $\text{pH} \leq 11.0$ is approximately equal. In fact, the conductivity of $\text{Ca}(\text{OH})_2$ solution was observed to be constant at $\text{pH} \leq 11.0$, up to a concentration of 15 mM. The results for 10 mM $\text{Ca}(\text{OH})_2$ solution at different pH is presented in Figure 4.29. The experimental data correlates with PHREEQC models, which calculates conductivity using the concentration and diffusion coefficient of the ionic species in the defined solution, and applies an ionic strength correction.

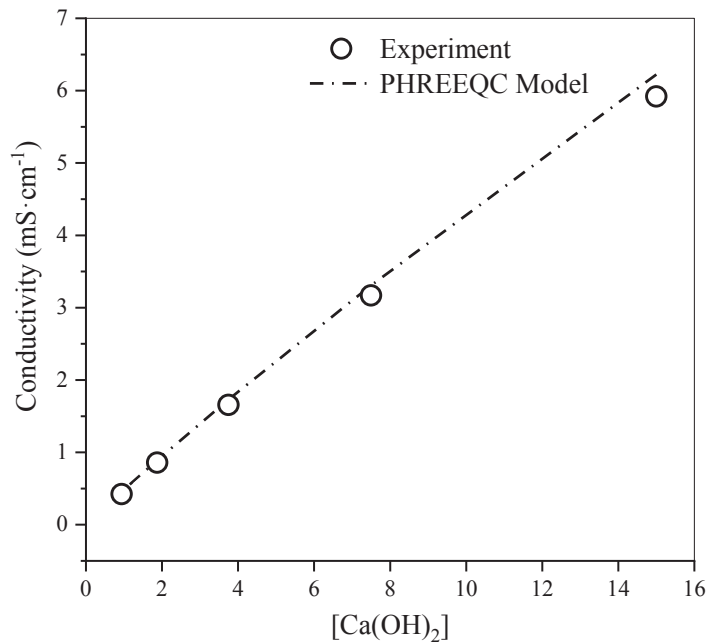


Figure 4.30. Relationship between $\text{Ca}(\text{OH})_2$ concentration and conductivity.

Since 50 mL of each precipitant was reacted during the process, neglecting the volume of HCl used, the final suspensions volume will be ~ 300 mL. For instance, when initial $\text{pH} \approx 12.5$, without considering the adsorption of Ca^{2+} ions on the particles, this treatment reduces the molar concentration of additive Ca^{2+} ions in the final suspension to ~ 6.7 mM, which has a conductivity of ~ 3 $\text{mS}\cdot\text{cm}^{-1}$ (Figure 4.30). However, Figure 4.28 shows the suspensions conductivity steadily decreased to a final value of ~ 3.5 $\text{mS}\cdot\text{cm}^{-1}$. This difference is considered an effect of the presence of Na^+ and Cl^- ions.

Figure 4.28 also shows the conductivity slightly decreased at pH = 12, but remained constant at pH = 11.5 and lower. Using the PHREEQC model, the conductivities of a 6.7 mM Ca(OH)₂ solution without pH adjustment, and at pH ≤ 11.0 were ~3 mS·cm⁻¹ and ~1.7 mS·cm⁻¹ respectively. However, the final suspensions conductivity at pH ≤ 11.0 was ~2.2 mS·cm⁻¹ (Figure 4.28). This suggests the presence of Na⁺ and Cl⁻ ions, and/or particle dissolution observed at low pH conditions, compensated for the gradual reduction in Ca²⁺ ions molarity in the solution and the expected spontaneous decrease in the suspensions conductivity.

Considering the stoichiometry of the reaction (Eq. 4.2), 50 mL of 25 mM CaCl₂ contains 1.25 mmol. This implies 2.5 mmol of Na⁺ and Cl⁻ ions would be present in the ~300 mL suspension at the end of the process. It is equivalent to a concentration of ~8.3 mM of NaCl solution which has a specific conductance of ~1 mS·cm⁻¹, which would have significantly affected the conductivity of the final suspension.

CHAPTER 5

CONCLUSION

The results show additive Ca^{2+} ions have remarkable effects on the growth, morphology, colloidal stability, specific surface area and crystal form of freshly-precipitated CaCO_3 particles. The ions adsorbed on the crystals, impeded their overgrowth and aggregation by enhancing electrostatic repulsions in the suspension.

The particles synthesized when $\text{Ca}(\text{OH})_2$ solution was replaced with pure H_2O were colloiddally unstable and polydisperse. The samples were a mixture of vaterite and calcite polymorph and contained particles as much as 20 times larger than the mean hydrodynamic size of particles obtained after growth inhibition in $\text{Ca}(\text{OH})_2$ solution.

In high alkaline conditions, the effects of the precipitants concentration and volume, and $\text{Ca}(\text{OH})_2$ concentration can be summed up as those of the concentration of additive Ca^{2+} ions available as growth inhibitors and the quantity of precipitated CaCO_3 particles. The ions lost their growth inhibitory efficiency at high precipitants concentration and precipitates volume.

Particles stability in the growth-inhibiting solution also diminished at higher precipitants concentration and volume. This is an outcome of the irreversible adsorption of additive Ca^{2+} ions on the first crystals growth sites, leaving lesser amounts for subsequent precipitates. It is also a probable effect of increased concentration of counter ions which weakened electrostatic repulsions necessary for colloidal stability.

The presence of the growth inhibiting Ca^{2+} ions engendered the crystallization of pure calcite particles, irrespective of the stabilizing solutions initial pH and precipitates residence time in the tubular reactor. Pure calcite phases were obtained both when only ACC was presumed to have precipitated in the tubular reactor, and when crystalline CaCO_3 was expected.

Even though the particles size increased as more precipitate was fed into the growth-inhibiting $\text{Ca}(\text{OH})_2$ solution, compared to the sizes of the particles obtained in the absence of additive Ca^{2+} ions, the described approach resulted in >90% growth inhibition. The extent to which it can be deployed is constrained by the limited solubility

of Ca(OH)_2 . Nonetheless, it is a simple procedure for the synthesis of stable monodisperse calcite nanoparticles at relatively high degrees of supersaturation.

No reaction among the ionic species was suspected in the solution. Changes in the growth-inhibiting solutions conductivity was observed to be the result of the increasing concentration of the precipitants counter ions and decreasing molar concentration of additive Ca^{2+} ions. Also, the difference between the initial and final suspensions pH were nominal.

Surface area analyses revealed additive Ca^{2+} ions also influenced the formation of pores in the particles. The porosity increased at higher Ca(OH)_2 concentration and low precipitates volume, but decreased as the growth-inhibiting solutions initial pH was lowered. Though the specific surface area reduced, the particles dissolved in low pH conditions and agglomerates of fragmented rhombohedra calcite particles were obtained.

The described approach can be used to produce calcite nanoparticles from conventional chemical precipitation reactions. However, it was observed that the solutions pH also contributes to the particles growth inhibition. High growth inhibition was obtained, only in the presence of additive Ca^{2+} ions and a high pH condition. Particles synthesized under this condition were porous and can be potentially used as adsorbents and carriers of small molecule compounds.

REFERENCES

1. Tai, C. Y.; Chen, F. B., Polymorphism of CaCO₃, precipitated in a constant-composition environment. *AIChE J.* **1998**, *44* (8), 1790-1798.
2. Naka, K.; Chujo, Y., Control of crystal nucleation and growth of calcium carbonate by synthetic substrates. *Chem. Mater.* **2001**, *13* (10), 3245-3259.
3. Cizer, Ö.; Rodriguez-Navarro, C.; Ruiz-Agudo, E.; Elsen, J.; Van Gemert, D.; Van Balen, K., Phase and morphology evolution of calcium carbonate precipitated by carbonation of hydrated lime. *Journal of Materials Science* **2012**, *47* (16), 6151-6165.
4. Ulkeryildiz, E.; Kilic, S.; Ozdemir, E., Rice-like hollow nano-CaCO₃ synthesis. *J. Cryst. Growth* **2016**, *450*, 174-180.
5. Njagic-Dzakula, B.; Falini, G.; Brecevic, L.; Skoko, Z.; Kralj, D., Effects of initial supersaturation on spontaneous precipitation of calcium carbonate in the presence of charged poly-L-amino acids. *J. Colloid Interface Sci.* **2010**, *343* (2), 553-63.
6. Bots, P.; Benning, L. G.; Rodriguez-Blanco, J.-D.; Roncal-Herrero, T.; Shaw, S., Mechanistic Insights into the Crystallization of Amorphous Calcium Carbonate (ACC). *Crystal Growth & Design* **2012**, *12* (7), 3806-3814.
7. Kontrec, J.; Ukrainczyk, M.; Džakula, B. N.; Kralj, D., Precipitation and characterization of hollow calcite nanoparticles. *Cryst. Res. Technol.* **2013**, *48* (9), 622-626.
8. Ogino, T.; Suzuki, T.; Sawada, K., The formation and transformation mechanism of calcium carbonate in water. *Geochim. Cosmochim. Acta* **1987**, *51* (10), 2757-2767.
9. Bolze, J.; Peng, B.; Dingenouts, N.; Panine, P.; Narayanan, T.; Ballauff, M., Formation and Growth of Amorphous Colloidal CaCO₃ Precursor Particles as Detected by Time-Resolved SAXS. *Langmuir* **2002**, *18* (22), 8364-8369.
10. Zebarjad, S. M.; Sajjadi, S. A., On the strain rate sensitivity of HDPE/CaCO₃ nanocomposites. *Materials Science and Engineering: A* **2008**, *475* (1-2), 365-367.
11. Lin, Y.; Chen, H.; Chan, C.-M.; Wu, J., High impact toughness polypropylene/CaCO₃ nanocomposites and the toughening mechanism. *Macromolecules* **2008**, *41* (23), 9204-9213.
12. Karakaş, F.; Hassas, B. V.; Celik, M. S., Effect of precipitated calcium carbonate additions on waterborne paints at different pigment volume concentrations. *Prog. Org. Coat.* **2015**, *83*, 64-70.
13. Hilder, M.; Batchelor, W., Surface-sensitive method to determine calcium carbonate filler contents in cellulose matrices. *Cellulose* **2010**, *17* (2), 407-415.

14. Trushina, D. B.; Bukreeva, T. V.; Kovalchuk, M. V.; Antipina, M. N., CaCO₃ vaterite microparticles for biomedical and personal care applications. *Mater Sci Eng C Mater Biol Appl* **2014**, *45*, 644-58.
15. Campos, J. S. d. C.; Ribeiro, A. A.; Cardoso, C. X., Preparation and characterization of PVDF/CaCO₃ composites. *Materials Science and Engineering: B* **2007**, *136* (2-3), 123-128.
16. Tas, A. C., Porous, Biphasic CaCO₃-Calcium Phosphate Biomedical Cement Scaffolds from Calcite (CaCO₃) Powder. *International journal of applied ceramic technology* **2007**, *4* (2), 152-163.
17. Vemula, P. K.; Anderson, R. R.; Karp, J. M., Nanoparticles reduce nickel allergy by capturing metal ions. *Nature nanotechnology* **2011**, *6* (5), 291.
18. Prepas, E. E.; Babin, J.; Murphy, T. P.; Chambers, P. A.; Sandland, G. J.; Ghadouani, A.; Serediak, M., Long-term effects of successive Ca(OH)₂ and CaCO₃ treatments on the water quality of two eutrophic hardwater lakes. *Freshwater biology* **2001**, *46* (8), 1089-1103.
19. Wei, W.; Ma, G.-H.; Hu, G.; Yu, D.; Mcleish, T.; Su, Z.-G.; Shen, Z.-Y., Preparation of hierarchical hollow CaCO₃ particles and the application as anticancer drug carrier. *J. Am. Chem. Soc.* **2008**, *130* (47), 15808-15810.
20. Ma, X.; Li, L.; Yang, L.; Su, C.; Guo, Y.; Jiang, K., Preparation of highly ordered hierarchical CaCO₃ hemisphere and the application as pH value-sensitive anticancer drug carrier. *Mater. Lett.* **2011**, *65* (19-20), 3176-3179.
21. Maleki Dizaj, S.; Barzegar-Jalali, M.; Zarrintan, M. H.; Adibkia, K.; Lotfipour, F., Calcium carbonate nanoparticles as cancer drug delivery system. *Expert opinion on drug delivery* **2015**, *12* (10), 1649-1660.
22. Wang, J.; Chen, J.-S.; Zong, J.-Y.; Zhao, D.; Li, F.; Zhuo, R.-X.; Cheng, S.-X., Calcium carbonate/carboxymethyl chitosan hybrid microspheres and nanospheres for drug delivery. *The Journal of Physical Chemistry C* **2010**, *114* (44), 18940-18945.
23. Liang, P.; Zhao, D.; Wang, C.-Q.; Zong, J.-Y.; Zhuo, R.-X.; Cheng, S.-X., Facile preparation of heparin/CaCO₃/CaP hybrid nano-carriers with controllable size for anticancer drug delivery. *Colloids and Surfaces B: Biointerfaces* **2013**, *102*, 783-788.
24. Gaumet, M.; Vargas, A.; Gurny, R.; Delie, F., Nanoparticles for drug delivery: the need for precision in reporting particle size parameters. *Eur J Pharm Biopharm* **2008**, *69* (1), 1-9.
25. Fu, S.-Y.; Feng, X.-Q.; Lauke, B.; Mai, Y.-W., Effects of particle size, particle/matrix interface adhesion and particle loading on mechanical properties of particulate-polymer composites. *Composites Part B: Engineering* **2008**, *39* (6), 933-961.
26. Meyer, H., The influence of impurities on the growth rate of calcite. *J. Cryst. Growth* **1984**, *66* (3), 639-646.

27. Kontrec, J.; Kralj, D.; Brečević, L.; Falini, G., Influence of some polysaccharides on the production of calcium carbonate filler particles. *J. Cryst. Growth* **2008**, *310* (21), 4554-4560.
28. Njegić-Džakula, B.; Brečević, L.; Falini, G.; Kralj, D., Calcite Crystal Growth Kinetics in the Presence of Charged Synthetic Polypeptides. *Crystal Growth & Design* **2009**, *9* (5), 2425-2434.
29. Cheng, B.; Lei, M.; Yu, J.; Zhao, X., Preparation of monodispersed cubic calcium carbonate particles via precipitation reaction. *Mater. Lett.* **2004**, *58* (10), 1565-1570.
30. Parakhonskiy, B. V.; Yashchenok, A. M.; Donatan, S.; Volodkin, D. V.; Tessarolo, F.; Antolini, R.; Möhwald, H.; Skirtach, A. G., Macromolecule Loading into Spherical, Elliptical, Star-Like and Cubic Calcium Carbonate Carriers. *ChemPhysChem* **2014**, *15* (13), 2817-2822.
31. Kilic, S.; Toprak, G.; Ozdemir, E., Stability of CaCO₃ in Ca(OH)₂ solution. *Int. J. Miner. Process.* **2016**, *147*, 1-9.
32. Wang, Y.; Moo, Y. X.; Chen, C.; Gunawan, P.; Xu, R., Fast precipitation of uniform CaCO₃ nanospheres and their transformation to hollow hydroxyapatite nanospheres. *J. Colloid Interface Sci.* **2010**, *352* (2), 393-400.
33. Wang, C., Control the polymorphism and morphology of calcium carbonate precipitation from a calcium acetate and urea solution. *Mater. Lett.* **2008**, *62* (16), 2377-2380.
34. Andreassen, J.-P., Formation mechanism and morphology in precipitation of vaterite—nano-aggregation or crystal growth? *J. Cryst. Growth* **2005**, *274* (1-2), 256-264.
35. Pouget, E. M.; Bomans, P. H.; Goos, J. A.; Frederik, P. M.; de With, G.; Sommerdijk, N. A., The initial stages of template-controlled CaCO₃ formation revealed by cryo-TEM. *Science* **2009**, *323* (5920), 1455-8.
36. Gebauer, D.; Volkel, A.; Colfen, H., Stable prenucleation calcium carbonate clusters. *Science* **2008**, *322* (5909), 1819-22.
37. Dupont, L.; Portemer, F., Synthesis and study of a well crystallized CaCO₃ vaterite showing a new habitus. *J. Mater. Chem.* **1997**, *7* (5), 797-800.
38. Nehrke, G.; Van Cappellen, P., Framboidal vaterite aggregates and their transformation into calcite: a morphological study. *J. Cryst. Growth* **2006**, *287* (2), 528-530.
39. Rodriguez-Blanco, J. D.; Shaw, S.; Benning, L. G., The kinetics and mechanisms of amorphous calcium carbonate (ACC) crystallization to calcite, via vaterite. *Nanoscale* **2011**, *3* (1), 265-71.
40. Rodriguez-Blanco, J. D.; Shaw, S.; Benning, L. G., How to make 'stable' ACC: protocol and preliminary structural characterization. *Mineralogical Magazine* **2018**, *72* (01), 283-286.

41. Boistelle, R.; Astier, J. P., Crystallization mechanisms in solution. *J. Cryst. Growth* **1988**, *90* (1-3), 14-30.
42. Kim, Y. Y.; Carloni, J. D.; Demarchi, B.; Sparks, D.; Reid, D. G.; Kunitake, M. E.; Tang, C. C.; Duer, M. J.; Freeman, C. L.; Pokroy, B.; Penkman, K.; Harding, J. H.; Estroff, L. A.; Baker, S. P.; Meldrum, F. C., Tuning hardness in calcite by incorporation of amino acids. *Nat Mater* **2016**, *15* (8), 903-10.
43. Cölfen, H., Precipitation of carbonates: recent progress in controlled production of complex shapes. *Current opinion in colloid & interface science* **2003**, *8* (1), 23-31.
44. Altay, E.; Shahwan, T.; Tanoğlu, M., Morphosynthesis of CaCO₃ at different reaction temperatures and the effects of PDDA, CTAB, and EDTA on the particle morphology and polymorph stability. *Powder Technol.* **2007**, *178* (3), 194-202.
45. Zhang, Q.; Ren, L.; Sheng, Y.; Ji, Y.; Fu, J., Control of morphologies and polymorphs of CaCO₃ via multi-additives system. *Mater. Chem. Phys.* **2010**, *122* (1), 156-163.
46. Ma, Z.; Mu, Y.; Shi, W.; Wang, J.; Liu, X.; Wang, X.; Dong, Z., HPAM–HABS induced synthesis of a labyrinth-like surface of calcite via rhombohedral lattice growth from the nanoscale. *CrystEngComm* **2018**, *20* (25), 3445-3448.
47. Yao, C.; Xie, A.; Shen, Y.; Zhu, J.; Li, H., Nacre-like calcium carbonate controlled by ionic liquid/graphene oxide composite template. *Mater Sci Eng C Mater Biol Appl* **2015**, *51*, 274-8.
48. Tang, H.; Yu, J.; Zhao, X., Controlled synthesis of crystalline calcium carbonate aggregates with unusual morphologies involving the phase transformation from amorphous calcium carbonate. *Mater. Res. Bull.* **2009**, *44* (4), 831-835.
49. Sand, K. K.; Rodriguez-Blanco, J. D.; Makovicky, E.; Benning, L. G.; Stipp, S. L. S., Crystallization of CaCO₃ in Water–Alcohol Mixtures: Spherulitic Growth, Polymorph Stabilization, and Morphology Change. *Crystal Growth & Design* **2011**, *12* (2), 842-853.
50. Blue, C. R.; Giuffre, A.; Mergelsberg, S.; Han, N.; De Yoreo, J. J.; Dove, P. M., Chemical and physical controls on the transformation of amorphous calcium carbonate into crystalline CaCO₃ polymorphs. *Geochim. Cosmochim. Acta* **2017**, *196*, 179-196.
51. Manoli, F.; Dalas, E., Spontaneous precipitation of calcium carbonate in the presence of ethanol, isopropanol and diethylene glycol. *J. Cryst. Growth* **2000**, *218* (2-4), 359-364.
52. Štajner, L.; Kontrec, J.; Njegić Džakula, B.; Maltar-Strmečki, N.; Plodinec, M.; Lyons, D. M.; Kralj, D., The effect of different amino acids on spontaneous precipitation of calcium carbonate polymorphs. *J. Cryst. Growth* **2018**, *486*, 71-81.
53. Reddy, M. M.; Hoch, A. R., Calcite Crystal Growth Rate Inhibition by Polycarboxylic Acids. *J. Colloid Interface Sci.* **2001**, *235* (2), 365-370.

54. Green, D. C.; Ihli, J.; Thornton, P. D.; Holden, M. A.; Marzec, B.; Kim, Y. Y.; Kulak, A. N.; Levenstein, M. A.; Tang, C.; Lynch, C.; Webb, S. E.; Tynan, C. J.; Meldrum, F. C., 3D visualization of additive occlusion and tunable full-spectrum fluorescence in calcite. *Nat Commun* **2016**, *7*, 13524.
55. Han, Y. S.; Hadiko, G.; Fuji, M.; Takahashi, M., Influence of initial CaCl₂ concentration on the phase and morphology of CaCO₃ prepared by carbonation. *Journal of materials science* **2006**, *41* (14), 4663-4667.
56. Song, R.-Q.; Cölfen, H., Additive controlled crystallization. *CrystEngComm* **2011**, *13* (5), 1249-1276.
57. Boyjoo, Y.; Pareek, V. K.; Liu, J., Synthesis of micro and nano-sized calcium carbonate particles and their applications. *Journal of Materials Chemistry A* **2014**, *2* (35), 14270-14288.
58. Guo, X. H.; Yu, S. H.; Cai, G. B., Crystallization in a mixture of solvents by using a crystal modifier: Morphology control in the synthesis of highly monodisperse CaCO₃ microspheres. *Angew. Chem. Int. Ed.* **2006**, *45* (24), 3977-3981.
59. Guo, X.; Liu, L.; Wang, W.; Zhang, J.; Wang, Y.; Yu, S.-H., Controlled crystallization of hierarchical and porous calcium carbonate crystals using polypeptide type block copolymer as crystal growth modifier in a mixed solution. *CrystEngComm* **2011**, *13* (6), 2054-2061.
60. Xu, A. W.; Antonietti, M.; Yu, S. H.; Cölfen, H., Polymer-Mediated Mineralization and Self-Similar Mesoscale-Organized Calcium Carbonate with Unusual Superstructures. *Adv. Mater.* **2008**, *20* (7), 1333-1338.
61. Zhao, Y.; Li, S.; Yu, L.; Liu, Y.; Wang, X.; Jiao, J., The preparation of calcium carbonate crystals regulated by mixed cationic/cationic surfactants. *J. Cryst. Growth* **2011**, *324* (1), 278-283.
62. Cölfen, H.; Qi, L., A systematic examination of the morphogenesis of calcium carbonate in the presence of a double-hydrophilic block copolymer. *Chemistry—A European Journal* **2001**, *7* (1), 106-116.
63. Ukrainczyk, M.; Kontrec, J.; Kralj, D., Precipitation of different calcite crystal morphologies in the presence of sodium stearate. *J. Colloid Interface Sci.* **2009**, *329* (1), 89-96.
64. Gutjahr, A.; Dabringhaus, H.; Lacmann, R., Studies of the growth and dissolution kinetics of the CaCO₃ polymorphs calcite and aragonite II. The influence of divalent cation additives on the growth and dissolution rates. *J. Cryst. Growth* **1996**, *158* (3), 310-315.
65. Mucci, A.; Morse, J. W., The incorporation of Mg²⁺ and Sr²⁺ into calcite overgrowths: influences of growth rate and solution composition. *Geochim. Cosmochim. Acta* **1983**, *47* (2), 217-233.

66. Reddy, M. M.; Wang, K. K., Crystallization of calcium carbonate in the presence of metal ions: I. Inhibition by magnesium ion at pH 8.8 and 25 C. *J. Cryst. Growth* **1980**, *50* (2), 470-480.
67. Jung, W.-M.; Hoon Kang, S.; Kim, K.-S.; Kim, W.-S.; Kyun Choi, C., Precipitation of calcium carbonate particles by gas–liquid reaction: Morphology and size distribution of particles in Couette-Taylor and stirred tank reactors. *J. Cryst. Growth* **2010**, *312* (22), 3331-3339.
68. Ulkeryildiz, E.; Kilic, S.; Ozdemir, E., Nano-CaCO₃ synthesis by jet flow. *Colloids and Surfaces A: Physicochemical and Engineering Aspects* **2017**, *512*, 34-40.
69. Parsons, R., The electrical double layer: recent experimental and theoretical developments. *Chem. Rev.* **1990**, *90* (5), 813-826.
70. Malvern, Zetasizer nano series user manual. 2009.
71. Thompson, P. A.; Troian, S. M., A general boundary condition for liquid flow at solid surfaces. *Nature* **1997**, *389* (6649), 360.
72. Moulin, P.; Roques, H., Zeta potential measurement of calcium carbonate. *J. Colloid Interface Sci.* **2003**, *261* (1), 115-126.
73. Chibowski, E.; Hotysz, L.; Szcześ, A., Time dependent changes in zeta potential of freshly precipitated calcium carbonate. *Colloids and Surfaces A: Physicochemical and Engineering Aspects* **2003**, *222* (1-3), 41-54.
74. Ukrainczyk, M.; Kontrec, J.; Babić-Ivančić, V.; Brečević, L.; Kralj, D., Experimental design approach to calcium carbonate precipitation in a semicontinuous process. *Powder Technol.* **2007**, *171* (3), 192-199.
75. Faatz, M.; Gröhn, F.; Wegner, G., Amorphous Calcium Carbonate: Synthesis and Potential Intermediate in Biomineralization. *Adv. Mater.* **2004**, *16* (12), 996-1000.
76. Pontoni, D.; Bolze, J.; Dingenouts, N.; Narayanan, T.; Ballauff, M., Crystallization of Calcium Carbonate Observed In-situ by Combined Small- and Wide-angle X-ray Scattering. *The Journal of Physical Chemistry B* **2003**, *107* (22), 5123-5125.
77. Bootz, A.; Vogel, V.; Schubert, D.; Kreuter, J., Comparison of scanning electron microscopy, dynamic light scattering and analytical ultracentrifugation for the sizing of poly(butyl cyanoacrylate) nanoparticles. *European Journal of Pharmaceutics and Biopharmaceutics* **2004**, *57* (2), 369-375.
78. Al Mahrouqi, D.; Vinogradov, J.; Jackson, M. D., Zeta potential of artificial and natural calcite in aqueous solution. *Adv. Colloid Interface Sci.* **2017**, *240*, 60-76.
79. de Leeuw, N. H.; Parker, S. C., Surface Structure and Morphology of Calcium Carbonate Polymorphs Calcite, Aragonite, and Vaterite: An Atomistic Approach. *The Journal of Physical Chemistry B* **1998**, *102* (16), 2914-2922.
80. Duckworth, O. W.; Martin, S. T., Dissolution rates and pit morphologies of rhombohedral carbonate minerals. *Am. Mineral.* **2004**, *89* (4), 554-563.

81. Vavouraki, A. I.; Putnis, C. V.; Putnis, A.; Koutsoukos, P. G., An atomic force microscopy study of the growth of calcite in the presence of sodium sulfate. *Chem. Geol.* **2008**, *253* (3-4), 243-251.
82. Rieger, J.; Frechen, T.; Cox, G.; Heckmann, W.; Schmidt, C.; Thieme, J., Precursor structures in the crystallization/precipitation processes of CaCO₃ and control of particle formation by polyelectrolytes. *Faraday Discuss.* **2007**, *136*, 265-277.
83. Kralj, D.; Brečević, L.; Kontrec, J., Vaterite growth and dissolution in aqueous solution III. Kinetics of transformation. *J. Cryst. Growth* **1997**, *177* (3-4), 248-257.
84. Zhou, G.-T.; Yao, Q.-Z.; Fu, S.-Q.; Guan, Y.-B., Controlled crystallization of unstable vaterite with distinct morphologies and their polymorphic transition to stable calcite. *Eur. J. Mineral.* **2010**, *22* (2), 259-269.
85. Agnihotri, R.; Mahuli, S. K.; Chauk, S. S.; Fan, L.-S., Influence of surface modifiers on the structure of precipitated calcium carbonate. *Industrial & engineering chemistry research* **1999**, *38* (6), 2283-2291.
86. Brečević, L.; Nöthig-Laslo, V.; Kralj, D.; Popović, S., Effect of divalent cations on the formation and structure of calcium carbonate polymorphs. *J. Chem. Soc., Faraday Trans.* **1996**, *92* (6), 1017-1022.
87. Jung, T.; Kim, W. S.; Choi, C. K., Effect of monovalent salts on morphology of calcium carbonate crystallized in Couette-Taylor reactor. *Crystal Research and Technology: Journal of Experimental and Industrial Crystallography* **2005**, *40* (6), 586-592.
88. Sheng Han, Y.; Hadiko, G.; Fuji, M.; Takahashi, M., Crystallization and transformation of vaterite at controlled pH. *J. Cryst. Growth* **2006**, *289* (1), 269-274.
89. Oral, Ç. M.; Ercan, B., Influence of pH on morphology, size and polymorph of room temperature synthesized calcium carbonate particles. *Powder Technol.* **2018**, *339*, 781-788.
90. Rodriguez-Blanco, J.; Shaw, S.; Bots, P.; Roncal-Herrero, T.; Benning, L., The role of pH and Mg on the stability and crystallization of amorphous calcium carbonate. *J. Alloys Compd.* **2012**, *536*, S477-S479.
91. Wray, J. L.; Daniels, F., Precipitation of Calcite and Aragonite. *J. Am. Chem. Soc.* **1957**, *79* (9), 2031-2034.
92. Somasundaran, P.; Agar, G., The zero point of charge of calcite. *J. Colloid Interface Sci.* **1967**, *24* (4), 433-440.
93. Volodkin, D. V.; Larionova, N. I.; Sukhorukov, G. B., Protein encapsulation via porous CaCO₃ microparticles templating. *Biomacromolecules* **2004**, *5* (5), 1962-1972.